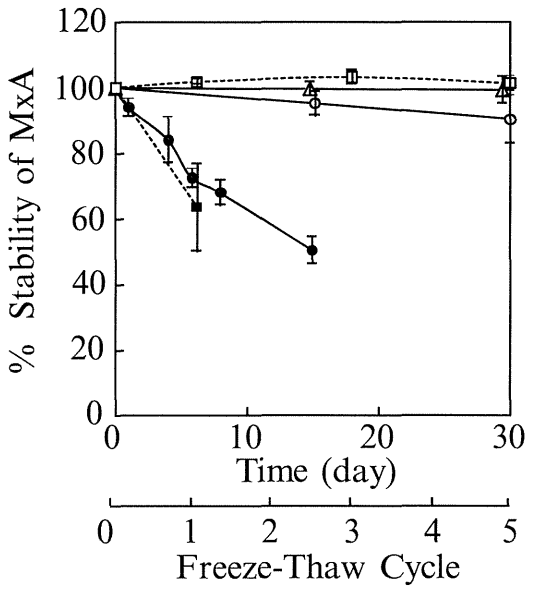

Fig. 5. Stability of MxA protein in whole blood.
–●–, stored at 4°C; –○– , treated with the dilution buffer and stored at 4°C; △ , treated with the dilution buffer and then stored at –80°C; ---■---, frozen and thawed; ---□---, treated with the dilution buffer and then frozen and thawed.

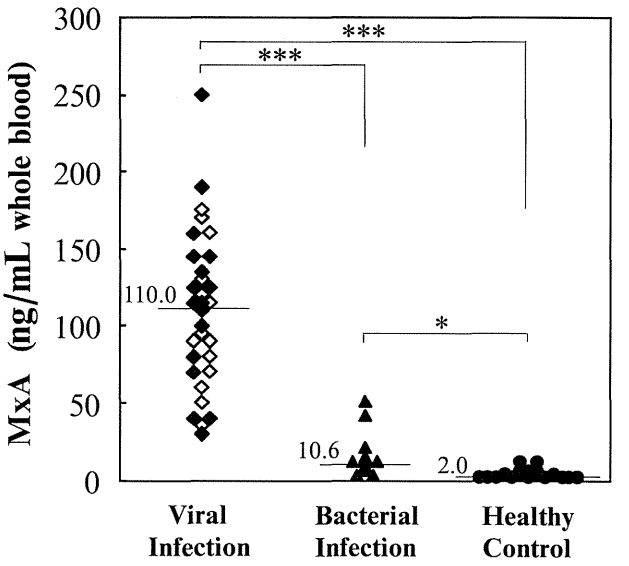

Fig. 6. MxA protein levels in whole blood of the healthy controls and patients with infection. ♦, patients with etiologically diagnosed viral infection; ◇, Patients with clinically diagnosed viral infection; ▲, patients with bacterial infection; •, healthy controls. Horizontal bars and values indicate the median for each group. $*P < 0.05$; $***P < 0.001$.

variation (CV) of each standard (range between 1.3 and 240 ng/ml) in whole blood was <10% (Fig. 4).

Assay Variation

The assay variation in the ELISA was examined using whole blood samples that contained MxA protein at three different concentrations (approximately 47 ng/ml, 105 ng/ml, and 193 ng/ml). The CV within assay and between assay were 2.0–5.5% ($n = 12$) and 2.2–7.2% ($n = 5$), respectively. To determine the analytical recovery, one volume of recombinant MxA protein (27 ng/ml and 114 ng/ml) was mixed with nine volumes of the whole blood samples containing 17, 37, and 81 ng/ml of MxA protein. Recoveries of MxA protein ranged from 93.0 to 95.0% (27 ng/ml, $n = 2$) and from 96.0 to 98.0% (114 ng/ml, $n = 2$), respectively.

Stability of MxA Protein

In this study, we used whole blood samples that had been freshly prepared. Figure 5 shows the stability of MxA protein in whole blood samples. Under refrigerated conditions, the MxA protein concentration in whole blood tended to decrease gradually. When untreated whole blood was frozen and then thawed, the MxA protein value in whole blood decreased beyond the limits of acceptability. On the other hand, when the whole blood was treated with the dilution buffer, MxA protein was stable even under refrigerated conditions. Additionally, MxA protein in diluted whole blood at –80°C was very stable for at least 3 years and freezing and thawing had no effects on the MxA protein value in the dilution buffer. Therefore, we suggest that samples for MxA protein assay are incubated with the dilution buffer immediately and then used for analysis or frozen at –80°C until needed.

Clinical Samples

The clinical performance of the present ELISA was assessed by assaying MxA protein in the whole blood of healthy controls and patients with viral infection and bacterial infection. Table 2 shows a summary of the clinical characteristics of the subjects. Significant differences in MxA protein levels, white blood cells (WBC), and C-reactive protein (CRP) were observed in the patients with viral infection compared to the healthy controls or the patients with bacterial infection. In all the groups, no significant correlations were observed between MxA protein and CRP.

Figure 6 shows the distribution of MxA protein values in the whole blood of the patients with viral infection, the patients with bacterial infection, and the healthy controls. ROC analysis was applied to the detection of the cut-off limits and then, clinical sensitivities and specificities were calculated at the cut-off limits. The MxA-specific ELISA had a sensitivity of 100% and a specificity of 100% for viral infection against healthy control and at a cut-off point of

TABLE 2. Clinical Characteristics of the Child Patients with Infection and the Healthy Control

		Viral infection			Bacterial infection	Healthy control
		Etiologically diagnosed	Clinically diagnosed	Total		
Number		17	14	31	11	18
Age	(Range)	0-10	0-6	0-10	0-6	5-11
	(Mean±SD)	2.35±2.99[c]	2.71±2.27[c]	2.52±2.66[c]	2.36±1.96[c]	7.50±1.75
Gender	(Male/Female)	6/11	8/6	14/17	8/3	12/6
MxA	(Median)	112.7[c,d]	91.7[c,d]	110.0[c,d]	10.6[c]	2.0
WBC	(Mean±SD)	10190±7175[d]	7270±1825[d]	8871±5575[d]	16352±10032	6599±1556[d]
CRP	(Median)	0.59[d]	0.49[d]	0.52[d]	7.42	0.08[d]
Final Diagnoses		RSV 10	Gastroenteritis 4		URI 5	
		Adenovirus 3	URI 10		UTI 3	
		Influenza virus A/B 3			Sepsis 2	
		Rotavirus 1			Pneumonia 1	

[a]Significantly different from the value of healthy control, $P < 0.05$.
[b]Significantly different from the value of bacterial infection, $P < 0.05$.
[c]Significantly different from the value of healthy control, $P < 0.0001$.
[d]Significantly different from the value of bacterial infection, $P < 0.0001$.
URI, upper respiratory infection; UTI, urinary tract infection.

36.7ng/ml, 87.1% and 90.9% for viral infection against bacterial infection, respectively.

DISCUSSION

The goal of this study was to develop an ELISA that met the requirements of a routine clinical assay for the measurement of MxA proteins in human whole blood.

The present ELISA is a sandwich-type assay developed using the mouse mAb KM1135 and KM1124. KM1135 recognized an epitope corresponding to the amino acids sequence of 10–220 of the human MxA protein GTP-binding domain and was used as the capture antibody. HRP-labeled KM1124 that recognized an epitope corresponding to the amino acids sequence of 221–297 was used as the secondary antibody. We selected mAb that reacted with the MxA protein GTP-binding domain, localized to the N-terminus and displayed an antivirus activity, all of which determined the specificity of the ELISA. We also checked that the mAb in this ELISA detected MxA protein in cells that was stimulated not only by interferon α but also influenza virus.

A rapid determination of MxA protein could be considered as a useful test in the diagnosis of viral disease. Towbin et al. prepared five mAb using recombinant MxA protein and they divided them into those that recognized an epitope corresponding to amino acids 1–429, and those which recognized another epitope corresponding to amino acids 430–662. They also developed a simple two-site immunometric enzyme assay with the mAb to measure MxA protein directly in blood (9). This method is simple and can measure intracellular MxA protein in whole blood, but took 20 h to perform the analysis. Oh et al. also developed a simple immunochemiluminescent assay for MxA protein (4) with the same mAb. They devised a method to reduce the time taken for analysis and to eliminate proteolytic degradation of MxA protein in whole blood lysate. However, the detection limit was 20 ng/ml in whole blood, which was insufficient to distinguish patients with viral infection from those with bacterial infection in the clinical setting.

Since MxA protein is highly susceptible to proteolysis, development of an assay system should consider eliminating any possibility of proteolytic degradation. Chieux et al. used denaturing media and heat-shock treatment to eliminate proteolytic degradation of MxA protein in blood lysate (6). In the present ELISA, we used the whole blood as a sample to measure MxA protein with the intention of developing a clinically significant and practical ELISA. As MxA protein is induced in white blood cells, the cells must be lysed before measuring MxA protein. Normally, NP-40 is used for the extraction of cytoplasmic proteins from cells. We used oleamide diethanolamide and 3-[(3-Cholamidopropyl) dimethylammonio] propanesulfonate in the dilution buffer to lyse the cells and to elute MxA protein from the cells. We checked the stability of MxA protein in various conditions by the ELISA, which detected the MxA protein GTP-binding domain of human MxA protein and found that our dilution buffer has a powerful effect on stability of the MxA protein. By using the dilution buffer for pretreatment of the whole blood, the stability of MxA protein was remarkable without the need for freezing, denaturing processes, or heat-shock treatment (6). Moreover, as freezing and thawing had also no effect on the MxA protein concentration

in the dilution buffer, samples for MxA protein measurement by the ELISA can be stored for long term at –80°C. When the whole blood was used for measuring MxA protein, high concentrations of hemoglobin were present in the sample and could interfere with the immunoreaction. Pretreatment of the whole blood with the dilution buffer also removed the interference of the hemoglobin. Additionally, the dilution buffer reduced the influence of variations in assay temperature on the assay results (data not shown). As long as we pretreated the whole blood with the dilution buffer, we could accurately measured MxA protein value in whole blood without proteolytic degradation, influence of assay condition, or interference from hemoglobin.

In this report, we demonstrated that the measurement of MxA protein in whole blood by the ELISA may be useful in the diagnosis of acute viral diseases. This assay is highly sensitive with a detection limit of 1.3 ng/ml MxA in whole blood and at 0.13 ng/ml in solution, which is sufficient to distinguish patients with viral infection from those with bacterial infections in the clinical setting. Due to the high sensitivity of the ELISA for measuring MxA protein, a sample could be pretreated and diluted 1/10 with the dilution buffer before assay. This pretreatment may remove interference from blood cell-based and plasma-based proteins and make it suitable for the routine measurement of MxA protein in human whole blood. The reproducibility and the accuracy of the ELISA are sufficient to measure MxA protein in whole blood. A total CV value of between 2.0 and 7.2% suggests this assay is very reproducible. In addition, the accuracy, as determined by the recovery of added MxA protein, is high enough for the measurement of clinical samples. This ELISA has a wide range of detection, corresponding to a clinically useful range of 1.3–240 ng/ml in whole blood. Highly purified recombinant human MxA protein was used as a standard and the use of this standard produced quantitative results in whole blood sample assays (Fig. 3).

As expected, the level of MxA protein detected in whole blood derived from patients with viral infection was significantly higher than that from healthy controls and from patients with a bacterial infection (Table 2, Fig. 6). At a cut-off point of 36.7 ng/ml, the present ELISA had a sensitivity of 87.1% and a specificity of 90.9% for viral infection against bacterial infection and the patients with viral infection were sharply distinguished from the healthy controls, that is, 100% of both a sensitivity and a specificity. The peripheral WBC count and serum CRP concentration have been used as markers to distinguish bacterial infection and viral infection. We observed that the peripheral WBC count and serum CRP concentration values were higher in the bacterial infection group compared to the viral infection group. However, the sensitivity and specificity of the MxA protein-specific ELISA was far higher than that of other markers tested, suggesting that it would be useful for the discrimination of patients with a viral infection.

It has been reported that many subjects received antibiotic treatment, despite their infections being viral in origin, and this inappropriate use of antibiotics is considered to be the main cause of the spread of multidrug-resistant bacteria (27). Several criteria have been proposed for identifying patients with bacterial infection (28–30). The present study shows that a whole blood assay for the MxA protein by the ELISA is useful for identifying the subjects whose illness is due to a viral infection. This ELISA might contribute toward a reduction in the number of unnecessary antibiotic prescriptions. However, the clinical study in this report was to assess the clinical performance of the MxA protein-specific ELISA. Further studies are necessary to establish the clinical use of the whole blood assay for MxA protein. In order to make the MxA assay more easily accessible in a clinical setting, we are pursuing the development of a rapid detection kit for MxA protein, using the same mAb and immunochromatography technology. This can detect MxA protein in whole blood within 15 min without the need for special equipment and we hope the kit will soon to be ready for clinical use.

In conclusion, we have developed a new assay, suitable for the measurement of MxA protein in human whole blood, which meets the requirements for routine clinical assay. The whole blood assay for MxA protein by the ELISA is useful for the identification of subjects who have a viral infection.

REFERENCES

1. Taylor JL, Grossberg SE. Recent progress on interferon research: Molecular mechanisms of regulation, action, and virus circumvention. Virus Res 1990;15:1–26.
2. Belardelli F. Role of interferon and other cytokines in the regulation of the immune response. APMIS 1995;103:161–179.
3. Kuzrrock R, Rosenblum MG, Sherwin AA, et al. Pharmacokinetics, single-dose tolerance, and biological activity of recombinant interferon-gamma in cancer patients. Cancer Res 1985;45:2866–2872.
4. Oh S-k, Luhowskyj S, Witt P, et al. Quantitation of interferon-induced Mx protein in whole blood lysates by an immunochemiluminescent assay: Elimination of protease activity of cell lysates in toto. J Immunol Methods 1994;176:79–91.
5. Sen CS, Lengyel P. A bird's eye view of its biochemistry. J Biol Chem 1992;267:5017–5020.
6. Chieux V, Hober D, Harvey J, et al. The MxA protein level in whole blood lysates of patients with various viral infections. J Virol Mehods 1998;70:183–191.
7. Horisberger MA. Interferon-induced human protein MxA is a GTPase which binds transiently to cellular proteins. Virology 1992;66:4705–4709.
8. von Wussow P, Jakschies D, Hochkeppel KH, Fibisch C, Penner L, Deicher H. The human intracellular Mx-homologous

protein is specifically induced by type I interferons. Eur J Immunol 1990;20:2015–2019.
9. Towbin H, Schmitz A, Jackschies D, von Wussow P, Horisberger MA. A whole blood immunoassay for the interferon-inducible human Mx protein. J Interferon Res 1992;12:67–74.
10. Ronni T, Melen K, Malygin A, Julkunen I. Control of IFN-inducible MxA gene expression in human cells. J Immunol 1993;150:1715–1718.
11. Simon A, Fäh J, Haller O, Staeheli P. Interferon-regulated Mx genes are not responsive to interleukin-1, tumor necrosis factor, and other cytokines. J Virol 1991;65:968–971.
12. Meier V, Mihm S, Ramadori G. MxA gene expression in peripheral blood mononuclear cells from patients infected chronically with hepatitis C virus treated with interferon-alpha. J Med Virol 2000;62:318–326.
13. Halminen M, Ilonen J, Julkunen I, Ruuskanen O, Simell O, Mäkelä MJ. Expression of MxA protein in blood lymphocytes discriminates between viral and bacterial infections in febrile children. Pediatr Res 1997;41:647–650.
14. Baca LM, Gems P, Kalvakolanu D, et al. Regulation of interferon-α-inducible cellular genes in human immunodeficiency virus-infected monocytes. J Leukocyte Biol 1994;55:299–309.
15. Jakschies D, Armbrust A, Clare KU, et al. Significant difference of the MxA-protein expression in human PBL of patients with viral and bacterial infections. J Interferon Res 1994;14:S124.
16. Haller O, Kochs G. Interferon-induced Mx proteins: Dynamin-like GTPases with antiviral activity. Traffic 2002;3:710–717.
17. Staeheli P, Haller O, Boll W, Lindenmann J, Weissmann C. Mx protein: Constitutive expression in 3T3 cells transformed with cloned Mx cDNA confers selective resistance to influenza virus. Cell 1986;44:147–158.
18. Zhao H, De BP, Das T, Banerjee AK. Inhibition of human parainfluenza virus-3 replication by interferon and human MxA. Virology 1996;220:330–338.
19. Schnorr JJ, Schneider-Schaulies S, Simon-Jodicke A, Pavlovic J, Horisberger MA, ter Meulen V. MxA-dependent inhibition of measles virus glycoprotein synthesis in a stably transfected human monocytic cell line. J Virol 1993;67:4760–4768.
20. Chieux V, Chehadeh W, Harvey J, Haller O, Wattre P, Hober D. Inhibition of coxsackievirus B4 replication in stably transfected cells expressing human MxA protein. Virology 2001;283:84–92.
21. Horisberger MA, McMaster G, Zeller H, Wathelet M, Dellis MG, Content J. Cloning and sequence analysis of cDNAs for interferon- and virus-induced human Mx-proteins reveal that they contain putative guanine nucleotide-binding site: Functional study of the corresponding gene promoter. J Virol 1990;64:1171–1181.
22. Kohno H, Sato S, Chiba H, et al. Monoclonal antibodies specific for 18-hydroxycortisol and their use in an enzyme immunoassay for human urinary 18-hydrocortisol for diagnosis of primary aldosteronism. Clin Biochem 1994;27:227–282.
23. Djavadi-Ohaniance L, Goldberg ME, Friguet B. Chapter 4. Measuring antibody affinity in solution. In: McCafferty J, editor. Antibody Engineering. Oxford: IRL Press; 1996. p 77–97.
24. Kohno H, Sueshige N, Oguri K, et al. Simple and practical sandwich-type enzyme immunoassay for human oxidatively modified low density lipoprotein using anti-oxidized phosphatidylcholine monoclonal antibody and anti-human apolipoprotein-B antibody. Clin Biochem 2000;33:243–253.
25. Bradford MM. Rapid and sensitive method for the quantitation of microgram quantities of protein utilizing the principle of protein-dye binding. Anal Biochem 1976;72:248–254.
26. Hanley JA, McNeil BJ. A method of comparing the areas under receiver operating characteristic curves derived from the same cases. Radiology 1983;148:839–843.
27. Huang N, Morlock L, Lee CH, Chen LS, Chou YJ. Antibiotic prescribing for children with nasopharyngitis (common colds), upper respiratory infections, and bronchitis who have health-professional parents. Pediatrics 2005;116:826–832.
28. Baker MD, Bell LM, Avner JR. Outpatient management without antibiotics of fever in selected infants. N Engl J Med 1993;329:1437–1441.
29. Baskin MN, O'Rourke EJ, Fleisher OR. 1992. Outpatient treatment of febrile infants 28 to 89 days of age with intramuscular administration of ceftriaxone. J Pediatr 120: 22–27.
30. Jaskiewicz JA, McCarthy CA, Richardson AC, et al. Febrile infants at low risk for serious bacterial infection-an appraisal of the Rochester criteria and implications for management. Febrile Infant Collaborative Study Group. Pediatrics 1994;94:390–396.

JVI
Journals.ASM.org

YB-1 Functions as a Porter To Lead Influenza Virus Ribonucleoprotein Complexes to Microtubules

Atsushi Kawaguchi,[a,b] Ken Matsumoto,[c,d] and Kyosuke Nagata[a]

Department of Infection Biology, Faculty of Medicine and Graduate School of Comprehensive Human Sciences, University of Tsukuba, Tsukuba, Japan[a]; Kitasato Institute for Life Sciences, Kitasato University, Tokyo, Japan[b]; Molecular Entomology Laboratory, RIKEN, Saitama, Japan[c]; and PRESTO, Japan Science and Technology Agency, Saitama, Japan[d]

***De novo*-synthesized RNAs are under the regulation of multiple posttranscriptional processes by a variety of RNA-binding proteins. The influenza virus genome consists of single-stranded RNAs and exists as viral ribonucleoprotein (vRNP) complexes. After the replication of vRNP in the nucleus, it is exported to the cytoplasm and then reaches the budding site beneath the cell surface in a process mediated by Rab11a-positive recycling endosomes along microtubules. However, the regulatory mechanisms of the postreplicational processes of vRNP are largely unknown. Here we identified, as a novel vRNP-interacting protein, Y-box-binding protein 1 (YB-1), a cellular protein that is involved in regulation of cellular transcription and translation. YB-1 translocated to the nucleus from the cytoplasm and accumulated in PML nuclear bodies in response to influenza virus infection. vRNP assembled into the exporting complexes with YB-1 at PML nuclear bodies. After nuclear export, using YB-1 knockdown cells and *in vitro* reconstituted systems, YB-1 was shown to be required for the interaction of vRNP exported from the nucleus with microtubules around the microtubule-organizing center (MTOC), where Rab11a-positive recycling endosomes were located. Further, we also found that YB-1 overexpression stimulates the production of progeny virions in an Rab11a-dependent manner. Taking these findings together, we propose that YB-1 is a porter that leads vRNP to microtubules from the nucleus and puts it into the vesicular trafficking system.**

In general, RNA transcripts form ribonucleoprotein (RNP) complexes with a number of RNA-binding proteins. The destiny of the RNP complexes in terms of localization, stability, and translational control is regulated by their protein constituents (16, 21, 33).

The genome of influenza type A viruses consists of eight-segmented and single-stranded RNAs of negative polarity (vRNA). vRNA exists as RNP complexes (designated vRNP) with viral RNA-dependent RNA polymerase consisting of three subunits (PB1, PB2, and PA) and nucleoprotein (NP). vRNA is transcribed into mRNA and replicated through cRNA (a full-size complementary copy of vRNA) into a large number of progeny vRNAs in the nucleus (reviewed in reference 49). The replicated vRNA is assembled into vRNP, and then the progeny vRNP interacts with M1. The vRNP-M1 complex is exported from the nucleus through the CRM1-dependent pathway mediated by the interaction of the vRNP-M1 complex with NS2 (also called NEP), which is a viral protein containing a nuclear export signal (NES) (19, 52, 54, 77). After the nuclear export, it is quite likely that the progeny vRNP accumulates in the microtubule-organizing center (MTOC) and then moves to the budding site beneath the cell surface along microtubules through Rab11a-dependent vesicular trafficking systems (28, 45). Finally, a set of eight segments of vRNA is incorporated into a progeny virion with other viral structural proteins (51, 53, 79).

The Rab11a-positive recycling endosome is important for the delivery of membranes and core polarity proteins to the lateral cell surface (reviewed in references 25, 42, and 74), leading to the construction of plasma membrane domains and epithelial cell polarity through binding to motor proteins along the cytoskeleton (75). The Rab11a-positive recycling endosome is typically located in close proximity to the nucleus and associated with the MTOC. Recent reports demonstrate that a number of viruses, including influenza virus (1, 17, 47), human cytomegalovirus (36), hantavirus (61), respiratory syncytial virus (6, 73), and Sendai virus (SeV) (9), employ the Rab11a-positive recycling endosomes during the egress. However, the targeting mechanism of cargo molecules, including influenza virus vRNP, to the Rab11a-positive recycling endosome is still poorly understood.

Since only one or two viral proteins are expressed from each segment, the virus has to hijack cellular functions/machineries consisting of numerous cellular proteins to achieve every infection process. Therefore, to understand the regulatory mechanism of the localization and intracellular transport of vRNP, identification and characterization of viral and cellular proteins involved in these processes are required. Here, we identified as a novel vRNP-interacting protein, Y-box-binding protein 1 (YB-1), a cellular protein that is involved in regulation of cellular transcription and translation (41). In the nucleus, YB-1 functions as a Y-box promoter element-binding transcription factor (34, 37, 41). However, a major portion of YB-1 localizes in the cytoplasm and regulates mRNA translation and degradation as a major component of cellular mRNA ribonucleoprotein (mRNP). A sudden translational arrest in response to a variety of stresses is accompanied by the formation of stress granules (SGs) and an increase in the number of mRNA-processing bodies (P-bodies) to reprogram gene expression posttranscriptionally (3). It is suggested that SGs are aggregates of translationally inactive mRNAs containing stalled

Received 21 February 2012 Accepted 24 July 2012
Published ahead of print 1 August 2012
Address correspondence to Kyosuke Nagata, knagata@md.tsukuba.ac.jp.

doi:10.1128/JVI.00453-12

translation initiation complexes, while P-bodies are mRNP aggregates with proteins involved in mRNA decay and translational repression (2, 21). YB-1 accumulates in these cytoplasmic structures (2) and acts as either a translational activator or inhibitor depending on its amount bound to the target mRNP (55). Therefore, it is proposed that YB-1 determines the fate of cellular mRNPs from their synthesis to destruction.

Here, we found that YB-1 translocates to the nucleus in response to influenza virus infection. The YB-1 imported into the nucleus accumulates in nuclear speckles (promyelocytic leukemia nuclear bodies [PML NBs]), together with vRNP, M1, and NS2 in the presence of leptomycin B (LMB), a potent inhibitor of CRM1, suggesting that YB-1 is associated with the vRNP export complexes in the nucleus. At late phases of infection, YB-1 was found in perinuclear granules with the newly synthesized vRNP and accumulated in Rab11a-positive recycling endosomes along microtubules. Further, we found that YB-1 mediates the interaction of vRNP with microtubules. Taking these findings together, we propose that YB-1 functions as a porter that facilitates the association of the progeny vRNP with microtubules, thereby leading the travel of vRNP onto Rab11a-positivie recycling endosomes.

MATERIALS AND METHODS

Biological materials. vRNP was prepared from purified influenza A/Puerto Rico/8/34 (A/PR/8/34) virus as previously described (66). Rabbit polyclonal antibodies against YB-1, RAP55, RCK, PB1, PB2, PA, M1, and NP and rat antibody against NS2 were prepared as previously described (30, 31, 40, 50, 71, 72, 77). Rabbit polyclonal antibodies against TIAR, PML (Santa Cruz Biotechnology), and Rab11a (Invitrogen) and mouse monoclonal antibodies against α-tubulin (Sigma) and PML (Santa Cruz Biotechnology) were purchased. Anti-SeV antibody and anti-M1 monoclonal antibody were generous gifts from A. Kato (National Institute of Infectious Diseases, Japan) and S. Hongo and K. Sugawara (Yamagata University), respectively. MDCK, 293T, and HeLa cells were grown in minimal essential medium (MEM) containing 10% fetal bovine serum. For the construction of plasmids expressing His-YB-1 and FLAG-α-tubulin, the cDNAs were amplified with primers 5′-GGAATTCCATA TGAGCAGCGAGGCCGAGACCCAGC-3′ and 5′-GAACCGCTCGAGC TCAGCCCCGCCCTGCTCAGCCTCGGGAG-3′ for YB-1 and with primers 5′-CGCCACCATGGACTACAAGGATGACGACGACAAGCAT ATGCGTGAGTGCATCTCC-3′ and 5′-CTATTAATACTCTTCACCCT CAT-3′ for α-tubulin, and cDNAs were reverse transcribed from HeLa total RNA using oligo(dT)$_{20}$ primer as a template. YB-1 cDNA was cloned into plasmid pET24b, and the resultant plasmid was then used as a template to amplify FLAG-YB-1 cDNA with primers 5′-GCCGCCACCATG GACTACAAGGATGACGACGACAAGCATATGAGCAGCGAGGCCGA-3′ and 5′-CCCGGATCCTATTACTCAGCCCCGCCCTG-3′. FLAG-YB-1 and FLAG-α-tubulin cDNAs were cloned into plasmid pCAGGS. The cDNA fragments of YB-1 deletion mutants were amplified with primers 5′-GCAGATATCATGAGCAGCGAGGCCGA-3′ and 5′-TGCGGAT CCCTACCATGGCCCGCCGGCAGGC-3′ for the A/P domain (amino acids [aa]1 to 50), 5′-GCAGATATCATGAGCAGCGAGGCCGA-3′ and 5′-TGCGGATCCTTAACCAGGACCTGTAACATT-3′ for the ΔA/B domain (aa 1 to 129), 5′-GCAGATATCGACAAGAAGGTCATCGCAA-3′ and 5′-CCCGGATCCTATTACTCAGCCCCGCCCTG-3′ for the ΔA/P domain (aa 51 to 324), and 5′-GCACCATGGGATATCGGTGTTCCAG TTCAAGGC-3′ and 5′-CCCGGATCCTATTACTCAGCCCCGCCCT G-3′ for the A/B domain (aa 130 to 324) and then cloned into plasmid pGEX-6P. To establish HeLa cell lines constitutively expressing either FLAG-YB-1 or FLAG-α-tubulin, HeLa cells transfected with pSV2-Neo and either pCAGGS-FLAG-YB-1 or pCAGGS-FLAG-α-tubulin were selected by growth in the presence of 1 mg/ml G418 for 2 weeks, and then the G418-resistant colonies were isolated. Recombinant His-YB-1 and glutathione *S*-transferase (GST)-fused deletion mutants of YB-1 were purified according to the manufacturer's protocol. In addition, to remove the bacterial RNA possibly bound to YB-1, we treated recombinant YB-1 with RNase A before purification.

LC-MS analysis. Molecular masses of trypsin-digested peptides from proteins coimmunoprecipitated with NP were calculated by liquid chromatography-coupled mass spectrometry (LC-MS) analysis (Thermo) after reduction and alkylation of cysteine residues. Assignment of observed ions was done with Mascot search software.

Cellular localization of viral RNAs and proteins. Indirect immunofluorescence assays and fluorescence *in situ* hybridization (FISH) assays were carried out as previously described (28). Briefly, cells infected with A/PR/8/34 at multiplicity of infection (MOI) of 10 were fixed with 1% paraformaldehyde (PFA) for 5 min and then prepermeabilized with 0.01% digitonin in phosphate-buffered saline (PBS) for 5 min on ice. After being washed with PBS, cells were fixed in 4% PFA for 10 min and permeabilized with 0.5% Triton X-100 in PBS for 5 min on ice. After incubation in PBS containing 1% bovine serum albumin (BSA) for 1 h, coverslips were incubated with each antibody for 1 h and then with Alexa Fluor 488- or 568-conjugated anti-rabbit, -rat, and -mouse IgG antibodies (Invitrogen). After the indirect immunofluorescence assays, FISH assays were performed using RNA probes complementary to the segment 1 vRNA and cRNA/mRNA. Images were acquired by confocal laser scanning microscopy (Zeiss). Each micrograph is a confocal section taken at the same level of focus among samples, so that nuclei were fully observed with a maximum diameter.

Immunoprecipitation. Infected cells cross-linked with 0.5% formaldehyde for 10 min at room temperature were lysed by sonication in a buffer containing 20 mM Tris-HCl (pH 7.9), 100 mM NaCl, 30 mM KCl, 0.1% NP-40, and 1 mM EDTA. The lysates were subjected to centrifugation at 12,000 × *g*, and the supernatant fractions were subjected to immunoprecipitation with antibodies where indicated. For detection of viral RNAs immunoprecipitated with YB-1 from infected cells, the immunoprecipitates were subjected to reverse cross-linking in a buffer containing 50 mM Tris-HCl (pH 7.9), 5 mM EDTA, 50 mM dithiothreitol (DTT), and 1% SDS for 45 min at 70°C. After reverse cross-linking, viral RNAs were purified by phenol-chloroform extraction followed by ethanol precipitation and then reverse transcribed with primers to determine the levels of vRNA (5′-GACGATGCAACGGCTGGTCTG-3′, which corresponds to the segment 5 cRNA between nucleotide sequence positions 424 and 444), cRNA (5′-AGTAGAAACAAGGGTATTTTTCTTTA-3′, which is complementary to the segment 5 cRNA between nucleotide sequence positions 1540 and 1565), and viral mRNA [oligo(dT)$_{20}$ for poly(A) tail]. The synthesized single-stranded cDNAs were subjected to quantitative real-time PCR analysis (Dice real-time thermal cycler system TP800; TaKaRa) with two specific primers, i.e., 5′-GACGATGCAACGGCTGGT CTG-3′, which corresponds to the segment 5 cRNA between nucleotide sequence positions 424 and 444, and 5′-AGCATTGTTCCAACTCCTTT-3′, which is complementary to the segment 5 cRNA between nucleotide sequence positions 595 and 614.

Gene silencing mediated by siRNA. Short interfering RNAs (siRNAs) against the *Rab11a* and *YB-1* genes were purchased from Invitrogen. Cells (5×10^5) were transfected with 30 pmol of siRNA using Lipofectamine RNA interference (RNAi) Max (Invitrogen) according to the manufacturer's protocol.

Reconstruction of vRNP-microtubule complex mediated by YB-1. Cellular tubulin and microtubule-associated proteins (MAPs) purified from bovine brain as previously described (67) were kindly provided by K. Mizumoto (Kitasato University). The purified tubulin proteins (40 μg) were assembled into microtubules by incubation at 37°C for 20 min in a buffer containing 50 mM piperazine-*N*,*N*′-bis(2-ethanesulfonic acid) (PIPES)-NaOH (pH 6.8), 1 mM EGTA, 5 mM $MgCl_2$, 20% glycerol, 1 mM GTP, and 20 μM paclitaxel (originally named taxol). The reconstituted microtubules were precipitated by centrifugation at 32,000 rpm at 20°C for 20 min in an SW55Ti rotor (Beckman) to remove the monomeric

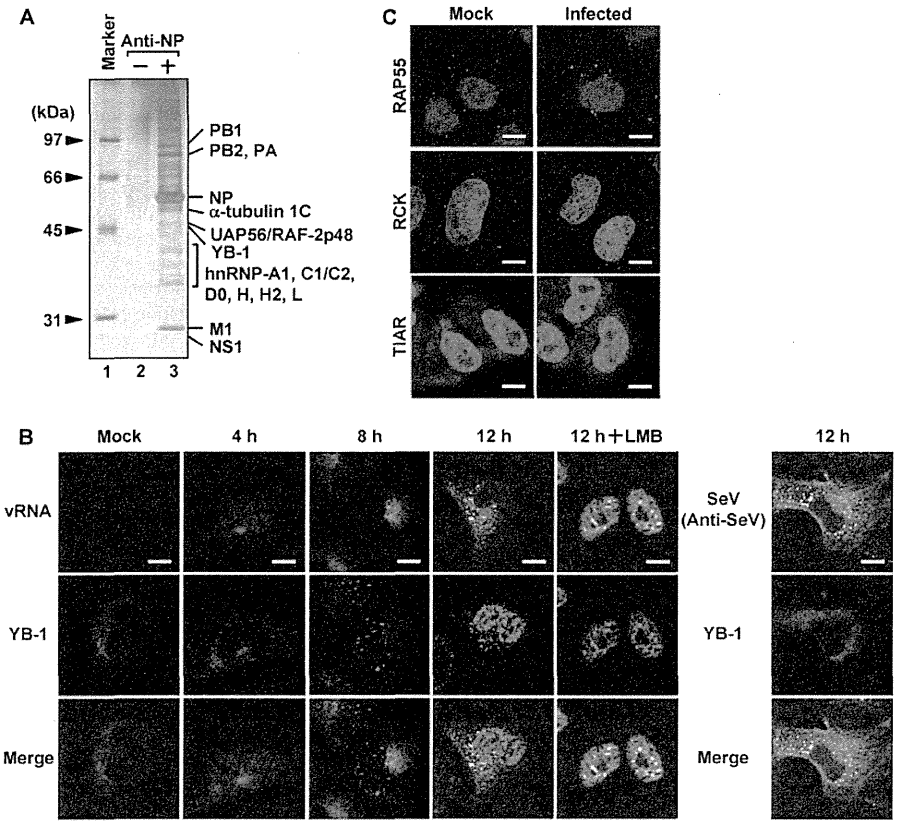

FIG 1 Identification of YB-1 as a novel vRNP-interacting proteins. (A) Identification of cellular and viral proteins interacting with vRNP complexes. HeLa cells infected with influenza virus at an MOI of 10 were subjected to immunoprecipitation assays with control IgG (lane 2) or anti-NP (lane 3) antibody-conjugated protein A-Sepharose. The coprecipitated proteins were eluted in 100 mM glycine (pH 2.8), separated through 10% SDS-PAGE, and visualized by silver staining. Molecular mass markers are also shown in lane 1. (B) Intracellular localization of YB-1 in infected cells. Infected MDCK cells were subjected to indirect immunofluorescence assays with anti-YB-1 antibody followed by FISH assays using a probe that hybridizes with segment 1 vRNA at 0, 4, 8, and 12 hpi. For LMB treatment, infected cells were incubated in culture medium containing 20 nM LMB at 7 hpi, and then the intracellular localization of vRNA and YB-1 was visualized by FISH and indirect immunofluorescence assays at 12 hpi. The result for SeV-infected cells at 12 hpi is also shown. Scale bars, 10 μm. (C) Intracellular localization of cellular proteins related to P-bodies and SGs. Mock-infected cells (left panels) or infected MDCK cells at 8 hpi (right panels) were subjected to indirect immunofluorescence assays with anti-RAP55 (upper panels, red), anti-RCK (middle panels, red), or anti-TIAR (lower panels, red) antibodies. Nuclear DNA was stained with TO-PRO-3 iodide (blue). Scale bars, 10 μm.

tubulin proteins. The precipitates were resuspended in a buffer containing 50 mM HEPES-NaOH (pH 7.9), 50 mM KCl, 20 μM paclitaxel, and 0.5% BSA and then incubated with either vRNP or YB-1-vRNP complexes. The vRNP complexes were immunoprecipitated with anti-NP antibody, and then the coprecipitated microtubules were detected by Western blotting assay with anti-α-tubulin antibody.

RESULTS

Identification of YB-1 as a novel vRNP-interacting protein. To gain further insight into the regulatory mechanism of vRNP function, we tried to identify a novel cellular protein(s) that interacts with vRNP. At 8 h postinfection (hpi), infected cell lysates were subjected to immunoprecipitation using anti-NP antibody, and then the precipitated proteins were subjected to LC-MS analysis (Fig. 1A). We found that viral proteins PB1, PB2, PA, M1, and NS1 were coprecipitated with NP, as expected (32, 39, 56, 58, 59), suggesting that not only NP but also vRNP was immunoprecipitated in this experiment. In addition to these viral proteins, we also identified a number of cellular proteins interacting with vRNP, as previously reported (Table 1) (29, 43, 44, 46, 76). It is noted that YB-1, a major component of cellular mRNP, was also identified as a novel vRNP-interacting protein. YB-1 regulates the lifetime and the translational activity of cellular mRNP, depending on the amount of YB-1 on a target mRNA (22, 55). Further, it is proposed that YB-1-bound mRNP particles interact with microtubules, but a precise role(s) of YB-1 has not yet been uncovered (11, 12). Thus, we tried to examine whether YB-1 regulates the fate of vRNP.

YB-1 localizes predominantly in the cytoplasm but translocates to the nucleus to regulate transcription in response to environmental stimuli such as DNA-damaging agents, UV irradiation, hyperthermia, and serum stimulation (34). More importantly, YB-1 is one of the components of SGs and P-bodies, which are cytoplasmic compartments possibly involved in the regulation of translation under stress conditions (78). Viral infection also gives a stressful environment to cells. To elucidate the biological significance of the interaction of vRNP with YB-1, we examined the

TABLE 1 LC-MS analysis of vRNP-interacting proteins

Protein	No. of observed peptides	Mascot score	Sequence coverage (%)
Heterogenous nuclear ribonucleoprotein A1	6	85	9
Heterogeneous nuclear ribonucleoproteins C1/C2	11	64	21
Heterogeneous nuclear ribonucleoprotein D0	4	77	12
Heterogeneous nuclear ribonucleoprotein H	9	159	17
Heterogeneous nuclear ribonucleoprotein H2	8	111	17
Heterogeneous nuclear ribonucleoprotein L	7	98	17
ATP-dependent RNA helicase DDX3Y	15	80	17
ATP-dependent RNA helicase DDX5	7	81	10
ATP-dependent RNA helicase DDX17	10	87	12
Nucleolin	8	85	13
78-kDa glucose-regulated protein	11	157	15
Importin subunit alpha 7	3	65	8
Y-box-binding protein 1	3	91	10
Tubulin alpha-1C chain	5	70	12
Spliceosome RNA helicase UAP56	5	62	10
Heat shock protein 90 alpha	9	111	15
Heat shock protein 90 beta	9	73	14
Heat shock cognate 71-kDa protein	11	134	15
Heat shock 70-kDa protein 1	12	120	14

intracellular localization of YB-1 in influenza virus-infected cells by indirect immunofluorescence assays using anti-YB-1 antibody (Fig. 1B). The vRNA was also counterstained by the fluorescence *in situ* hybridization (FISH) method (28). YB-1 localized at the cytoplasm in infected cells at 4 hpi, as it did in mock-infected cells. Along with the progression of infection, YB-1 was imported to the nucleus and accumulated in unknown nuclear speckles at 8 hpi. At 12 hpi, a portion of YB-1 was found in unknown cytoplasmic granules with the exported progeny vRNA. Since these cytoplasmic granules of YB-1 were not found in the presence of LMB, a potent inhibitor of CRM1, it is likely that YB-1 is exported with vRNA from the nucleus (Fig. 1B). Furthermore, the translocation of YB-1 upon influenza virus infection may not be involved in the innate immunity, since the localization of YB-1 was not changed in Sendai virus-infected cells (Fig. 1B). Next, we examined the intracellular localization of RAP55, RCK/p54, and TIAR proteins, which are components of cellular mRNP and accumulate in SGs and P-bodies (2). In contrast to the case for YB-1, we did not find any localization changes of these proteins in response to infection (Fig. 1C). Thus, the translocation of YB-1 found in infected cells may not be involved in a function as a component of SGs and P-bodies.

Interaction of YB-1 with vRNP-exporting complexes. Progeny vRNP is exported to the cytoplasm from the nucleus through the CRM1-dependent pathway by assembling export complexes with viral proteins M1 and NS2 (19, 52, 54, 77). Since YB-1 may be exported to the cytoplasm together with vRNP, it is assumed that YB-1 interacts with vRNP export complexes in the nucleus. To address this, we examined the colocalization of YB-1 with M1 and NS2. We found that M1 but not NS2 accumulated in the nuclear speckles with YB-1 at 8 hpi (Fig. 2A). Since a major portion of the progeny vRNA and NS2 was localized in the cytoplasm (Fig. 1B and 2A), the newly synthesized vRNP may be exported to the cytoplasm immediately after formation of the export complex. Thus, we examined the localization of vRNA and NS2 in LMB-

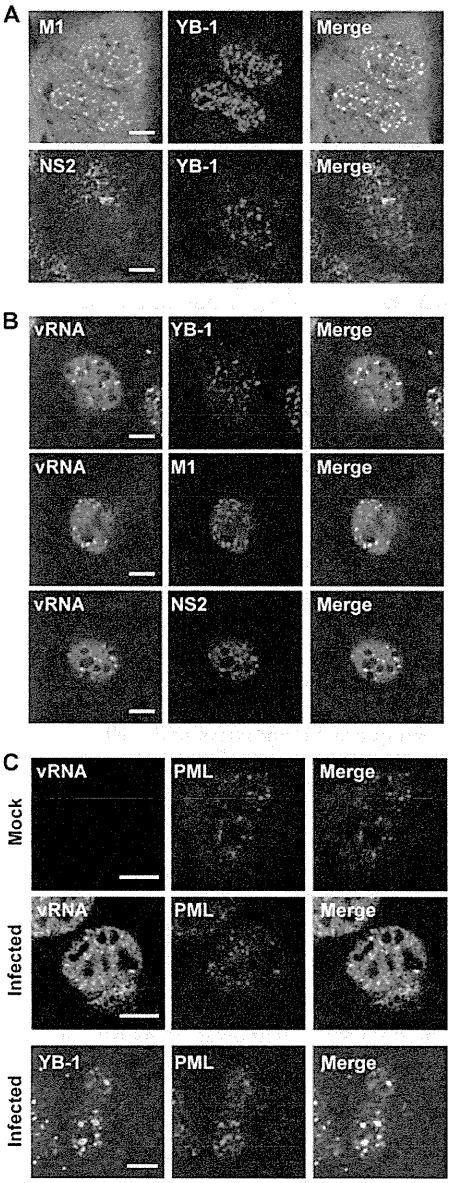

FIG 2 Colocalization of YB-1 and vRNP export complexes in nuclear speckles. (A) Intracellular localization of YB-1, M1, and NS2. At 8 hpi, infected MDCK cells were subjected to indirect immunofluorescence assays with rabbit anti-YB-1 (red) and either mouse anti-M1 (upper panel, green) or rat anti-NS2 (lower panel, green) antibody. Scale bar, 10 μm. (B) Intracellular localization of vRNA, YB-1, M1, and NS2 in the presence of LMB. At 7 hpi, infected MDCK cells were incubated for 1 h in the presence of 20 nM LMB. Segment 1 vRNA (left panels, green), YB-1 (upper panel, red), M1 (middle panel, red), and NS2 (lower panel, red) were visualized by FISH and indirect immunofluorescence assays. Scale bars, 10 μm. (C) Accumulation of vRNA and YB-1 in PML NBs in the presence of LMB. After treatment of LMB as described for panel B, mock-infected (upper panel) and infected (middle and lower panels) MDCK cells were subjected to FISH assays using the probe that hybridizes with segment 1 vRNA (upper and middle panels, green) and to indirect immunofluorescence assays with rabbit (upper and middle panels, red) and mouse (lower panel, red) anti-PML and rabbit anti-YB-1 antibodies (lower panel, green). Scale bars, 10 μm.

treated cells. Upon inhibition of the CRM1-dependent export pathway, vRNA accumulated in the nuclear speckles with YB-1, M1, and NS2 (Fig. 2B). Previously, it was reported that a small portion of M1 and NS2 may localize in PML NBs (62, 64). It has been shown that the overexpression of PML suppresses influenza virus proliferation (10, 27), suggesting that PML NBs may contribute to the cellular antiviral response. However, the role of PML NBs remains controversial, since influenza virus replicates normally in cells lacking the *PML* gene (20). As expected, in the presence of LMB, we found that vRNA and YB-1 were partially associated with PML NBs (Fig. 2C). Taking these findings together, it is possible that the YB-1 imported into the nucleus interacts with the vRNP export complexes in PML NBs and then YB-1 is subsequently exported from the nucleus with vRNP.

Influenza virus produces three different RNAs, i.e., vRNA, cRNA, and viral mRNA. Both vRNA and cRNA form ribonucleoprotein complexes with the viral polymerase and NP, whereas vRNA, but not cRNA, is found in the cytoplasm (26) and packaged into the virions. In contrast, the viral mRNA interacts with cellular mRNA-binding proteins and is exported through the REF/Aly pathway generally used by cellular mRNAs (4, 57). To examine the specific interaction of YB-1 with viral RNAs, we visualized positive-sense RNAs (cRNA and viral mRNA) by FISH assays. The intracellular localization of positive-sense RNAs was not changed by LMB treatment, as previously reported (57), and the FISH signals were not colocalized with YB-1 in the absence or presence of LMB (Fig. 3A). Further, to show quantitative results, we performed immunoprecipitation assays with cell lysates prepared from cells constitutively expressing FLAG-YB-1 using anti-FLAG antibody as described in Materials and Methods. We found that vRNA interacted with YB-1, but neither cRNA nor viral mRNA did in infected cells (Fig. 3B). Thus, it is quite likely that YB-1 is involved in the functional regulation of vRNP but not in that of either cRNP or viral mRNP.

Interaction of the YB-1-vRNP complex with Rab11a-positive recycling endosomes along microtubules. At 12 hpi, YB-1 was partially colocalized with the vRNA exported from the nucleus in the cytoplasm (Fig. 1B). Recent studies have suggested that the progeny vRNP is transported to the plasma membrane along microtubules via Rab11a-positive recycling endosomes (1, 17, 47). Further, it has been reported that YB-1 interacts with microtubules (12). Based on these findings, we examined whether YB-1 accumulates in microtubules with vRNP (Fig. 4). We found that the cytoplasmic punctate signals of YB-1 in perinuclear regions were colocalized with α-tubulin (Fig. 4A). We then examined the interaction of YB-1 with microtubules, Rab11a, and vRNP by immunoprecipitation assays. YB-1 interacted with α-tubulin but hardly with Rab11a in mock-infected cells (Fig. 4B, lane 3). In contrast, the interaction of YB-1 with Rab11a was significantly increased in infected cells (Fig. 4B, lane 6). To address whether the vRNP-YB-1 complexes accumulate in microtubules with Rab11a, the proteins coprecipitated with YB-1 from infected lysates (Fig. 4B, lane 6) were eluted and then subjected to reimmunoprecipitation with anti-NP antibody (Fig. 4C). Since α-tubulin and Rab11a were immunoprecipitated with anti-NP antibody (Fig. 4C, lane 3), it is quite likely that the progeny vRNP is accumulated on Rab11a-positive recycling endosomes with YB-1 along microtubules.

YB-1 is a positive factor for Rab11a-dependent virus production. It has been shown that Rab11a is required for the transport of

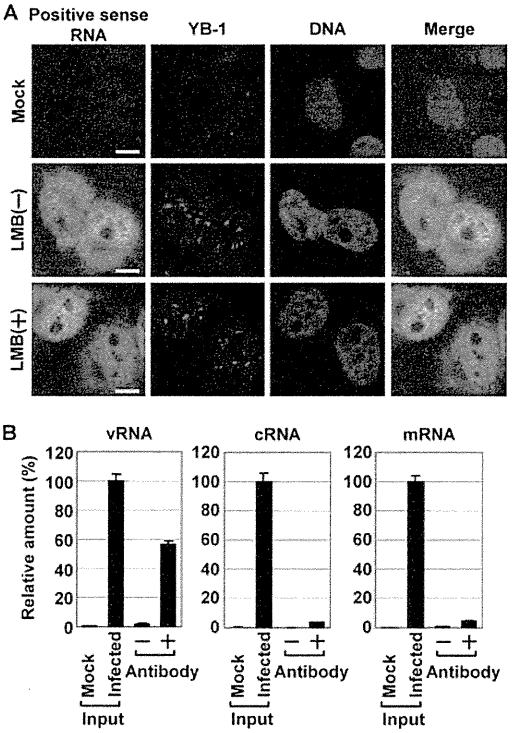

FIG 3 Specific interaction of YB-1 with vRNA but not with either cRNA or viral mRNA. (A) Intracellular localization of YB-1 and viral mRNA/cRNA. At 8 hpi, infected MDCK cells were subjected to FISH assays using a probe that hybridizes with segment 1 cRNA and mRNA (green) and to indirect immunofluorescence assays with anti-YB-1 antibody (red) with or without 20 nM LMB treatment for 1 h. Nuclear DNA was stained with TO-PRO-3 iodide (blue). Scale bars, 10 μm. (B) Coimmunoprecipitation of YB-1 and viral RNA molecules. HeLa cells constitutively expressing FLAG-YB-1 were infected with influenza virus at an MOI of 10. After 8 hpi, cell lysates were prepared and subjected to immunoprecipitation assays in the presence of either control IgG or anti-FLAG antibody as described in Materials and Methods. The immunoprecipitated viral RNAs were eluted with 100 μg/ml FLAG peptide and then quantitatively analyzed by reverse transcription followed by real-time PCR with primers specific for segment 5 vRNA, cRNA, and NP mRNA. To quantitatively evaluate the data, 5% equivalents of mock-infected and infected samples were also observed.

vRNP to the apical plasma membrane and thereby affects the production of progeny virions (1, 17, 47). Since YB-1 binds to Rab11a together with vRNP (Fig. 4C), it is assumed that YB-1 is involved in production of progeny virions through the Rab11a-positive recycling endosome pathway. To address this, the effect of YB-1 overexpression on the virus titer was examined using siRNA-mediated Rab11a knockdown (KD) cells (Fig. 5). The transfection efficiency was approximately 60%. The amount of exogenously overexpressed FLAG-YB-1 was 3-fold higher than that of endogenous YB-1, and the expression level of Rab11a in KD cells decreased to approximately 30% of that in control cells transfected with the nontargeting siRNA (Fig. 5A). The expression level of viral proteins was found to be virtually unchanged by YB-1 overexpression (Fig. 5B). We found that the amount of infectious virions produced from cells overexpressing YB-1 was significantly increased compared to that produced from cells transfected with empty plasmid, whereas the virus titer was slightly enhanced by

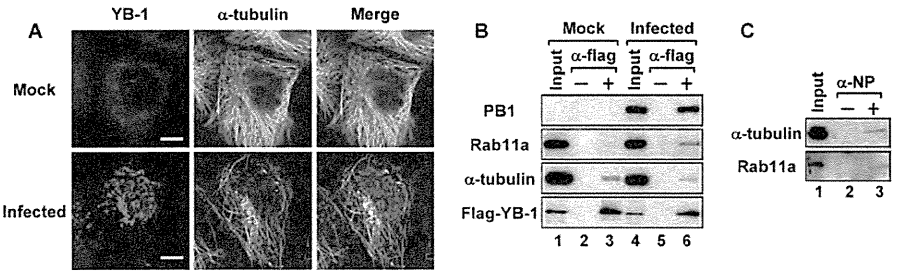

FIG 4 Accumulation of YB-1-vRNP complexes on microtubules with Rab11a-positive recycling endosomes in response to infection. (A) Colocalization of YB-1 and microtubules in cytoplasmic punctate signals. At 12 hpi, mock-infected (upper panels) and infected (lower panels) MDCK cells were subjected to indirect immunofluorescence assays with anti-YB-1 (red) and α-tubulin (green) antibodies. Scale bars, 10 μm. (B and C) Interaction of YB-1 with Rab11a-positive recycling endosomes on microtubules. HeLa cells constitutively expressing FLAG-YB-1 were infected with influenza virus at an MOI of 10. (B) Cell lysates were prepared and subjected to immunoprecipitation assays in the presence of either control IgG (lanes 2 and 5) or anti-FLAG antibody (lanes 3 and 6) at 12 hpi. Coprecipitated proteins were eluted with 100 μg/ml FLAG peptide and detected by Western blotting assays with anti-PB1, anti-Rab11a, anti-α-tubulin, and anti-FLAG antibodies. Ten percent equivalents of mock-infected (lane 1) and infected (lane 4) lysates were also subjected to Western blotting assays. (C) The eluate purified from infected lysate from panel B, lane 6, was reimmunoprecipitated with either control IgG (lane 2) or anti-NP antibody (lane 3), and then the eluate was subjected to Western blotting assays with anti-α-tubulin and anti-Rab11a antibodies. Lane 1, 30% equivalent of proteins immunopurified with anti-FLAG antibody from infected cell lysate.

YB-1 overexpression in Rab11a KD cells (Fig. 5C). Further, the slopes of the lines in Fig. 5C were determined to compare the efficiencies of virus production (Fig. 5D). This result shows that the production of infectious viruses was increased 4.8-fold by the YB-1 overexpression, but the stimulatory activity of YB-1 was reduced 1.9-fold by Rab11a KD (Fig. 5D). Therefore, it is concluded that YB-1 stimulates the production of infectious viruses in an Rab11a-dependent manner. We also tried to measure the amount of infectious virions produced from YB-1 KD cells. However, YB-1 KD cells tend to die from influenza virus infection after 16 to 20 hpi (data not shown). Thus, it was difficult to demonstrate the effect of YB-1 on the virus titer using YB-1 siRNA.

YB-1 functions as a porter for vRNP to direct it to microtubules. Figures 4 and 5 suggested that YB-1 functions in the vRNP transport through the Rab11a-positive recycling endosome pathway along microtubules. Next, we tried to demonstrate whether YB-1 functions as a transporter of vRNP to microtubules using siRNA-mediated gene silencing (Fig. 6). At 48 h after transfection of YB-1 siRNA, the expression level of YB-1 in KD cells decreased to 25% of that in control cells (Fig. 6A). There were no differences found in the accumulation levels of viral proteins (Fig. 6B) and vRNA and viral mRNA (Fig. 6C) between control and YB-1 KD cells. Previous reports showed that the vRNP complexes exported from the nucleus accumulate at the MTOC around the perinucleus (45) with Rab11a-positive recycling endosomes (1, 17, 47). We carried out FISH assays to examine whether vRNP complexes localize around the perinucleus in YB-1 KD cells at 8 hpi (Fig. 6D and E). A major population of YB-1 KD cells (81.5% ± 7.2%) had vRNA in a diffusive pattern. Thus, it is quite likely that YB-1 stimulates the accumulation of vRNP at the MTOC. As shown in Fig. 2C, the replicated vRNA associated with PML NBs in the presence of LMB. Since vRNA accumulated in PML NBs even in YB-1 KD cells with LMB treatment (Fig. 6D), it is strongly suggested that YB-1 is not involved in the association between vRNP and PML NBs. It is reported that exogenously expressed M1 is localized in PML NBs (64), suggesting that vRNP might accumulate in PML NBs through the interaction between vRNP and M1. It is also suggested that YB-1 does not play a role in the vRNP export from the nucleus to the cytoplasm, since vRNA was found predominantly in the cytoplasm of YB-1 KD cells (Fig. 6E).

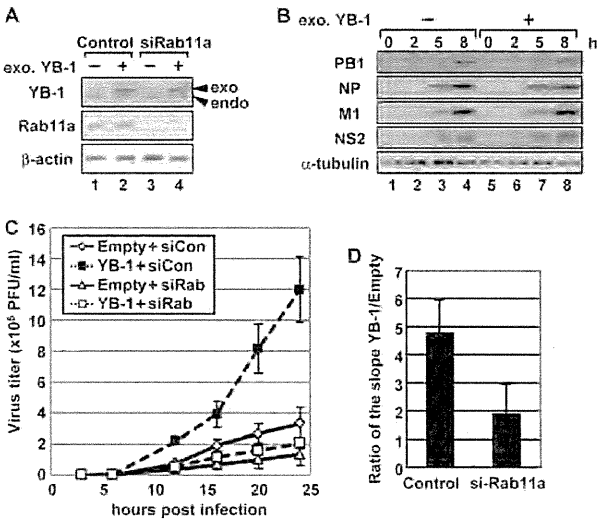

FIG 5 Effect of YB-1 overexpression on the production of infectious virions. (A) Expression levels of YB-1 and Rab11a proteins. 293T cells were transfected with either pCAGGS empty plasmid (lanes 1 and 3) or pCAGGS-FLAG-YB-1 (lanes 2 and 4) at 24 h after treatment of either nontargeting (control; lanes 1 and 2) or Rab11a (siRab11a; lanes 3 and 4) siRNA. At 24 h after transfection of expression vectors, the cell lysates were prepared and analyzed by SDS-PAGE followed by Western blotting assays with anti-YB-1, anti-Rab11a, and anti-β-actin antibodies. (B) Accumulation levels of viral proteins in cells overexpressing FLAG-YB-1. 293T cells were transfected with either pCAGGS or pCAGGS-FLAG-YB-1. At 24 h posttransfection, cells were infected with influenza virus at an MOI of 10. At 0, 2, 5, and 8 hpi, cell lysates were prepared and analyzed by Western blotting assays with anti-PB1, anti-NP, anti-M1, anti-NS2, and anti-α-tubulin antibodies. (C) Production of infectious virions. Control (open diamonds and filled squares) and Rab11a KD 293T (open triangles and open squares) cells transfected with either pCAGGS (open diamonds and open triangles) or pCAGGS-FLAG-YB-1 (filled and open squares) as described for panel A were infected with influenza virus at an MOI of 0.5. The culture supernatants collected at 3, 6, 12, 16, 20, and 24 hpi were subjected to plaque assays to examine the production of infectious virions in a single-round infection. The average titers and standard deviations determined from three independent experiments are shown. (D) Stimulatory activity of YB-1 on the virus titer in Rab11a KD cells. The slopes of the lines in panel C were determined by the least-squares method, and the ratio of the virus titer from cells overexpressing FLAG-YB-1 to that from cells transfected with pCAGGS is shown.

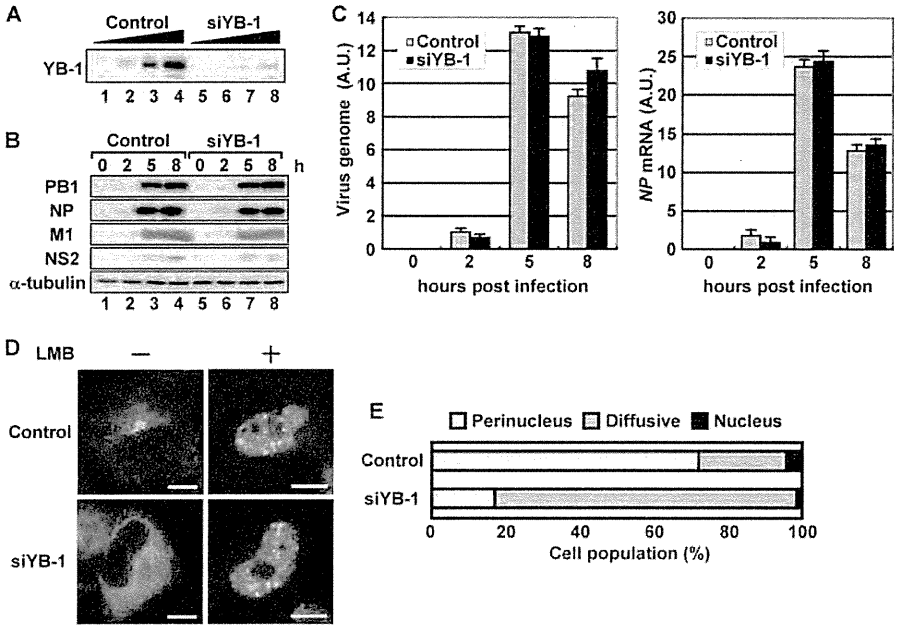

FIG 6 Accumulation of vRNP on microtubules in YB-1 knockdown cells. (A) Expression level of YB-1 in YB-1 KD cells. HeLa cells transfected with nontargeting (control; lanes 1 to 4) or YB-1 (siYB-1; lanes 5 to 8) siRNA were lysed, and then the lysates (2.5×10^3, 5×10^3, 1×10^4, and 2×10^4 cells) were subjected to SDS-PAGE followed by Western blotting assays with anti-YB-1 antibody at 48 h posttransfection. (B and C) Accumulation levels of viral proteins and RNAs in YB-1 KD cells. At 48 posttransfection of siRNA, control and YB-1 KD cells were infected with influenza virus at an MOI of 10. At 0, 2, 5, and 8 hpi, cell lysates were prepared and analyzed by Western blotting assays with anti-PB1, anti-NP, anti-M1, anti-NS2, and anti-α-tubulin antibodies. Total RNAs purified from the cells at 0, 2, 5, and 8 hpi were subjected to reverse transcription followed by quantitative real-time PCR with primers specific for segment 5 vRNA and NP mRNA as described in Materials and Methods. (D and E) Intracellular localization of vRNA in YB-1 KD cells. At 8 hpi with or without LMB treatment for 1 h, infected control and YB-1 KD cells were subjected to FISH assays using a probe that hybridizes with segment 1 vRNA (panel D) (scale bars, 10 μm). Cells were counted, and the localization pattern of vRNA in the absence of LMB was determined (E). The number of cells showing each localization pattern was expressed as the percentage of the total cell number ($n = 80$) in panel E. The average percentages determined from three independent experiments are shown.

YB-1 interacts with vRNP (Fig. 1A and 4B), but it is unclear whether YB-1 interacts directly with one or more vRNP components, that is, viral polymerase complexes, NP, and vRNA. To test this, we performed pulldown assays with purified vRNP and His-YB-1 using Ni-nitrilotriacetic acid (NTA) resin (Fig. 7A). Not only viral polymerase subunits but also NP was coprecipitated with YB-1 (lane 6), demonstrating that YB-1 interacts directly with vRNP. Since YB-1 has a single-stranded RNA binding activity, it is possible that YB-1 binds to vRNA. To address this, vRNP treated with micrococcal nuclease (mnRNP) to deplete vRNA was also subjected to the pulldown assay with His-YB-1. We found that each viral polymerase subunit but not NP from mnRNP was coprecipitated with YB-1 (Fig. 7A, lane 9), suggesting that YB-1 interacts with viral polymerase complexes. YB-1 consists of three domains: the N-terminal domain, the cold shock domain (CSD), and the C-terminal tail domain. The CSD has the well-characterized RNA-binding motifs RNP-1 and RNP-2 and thereby functions as a nucleic acid-binding domain. The N-terminal domain is rich in alanine and proline (A/P domain), and the C-terminal domain contains alternating clusters of positively and negatively charged amino acid residues (A/B domain). All three domains are involved in interaction with a number of cellular proteins (reviewed in reference 18). To further characterize the interaction between YB-1 and vRNP, we carried out pulldown assays with GST-fused deletion mutants of YB-1 and vRNP (Fig, 7B). We found that PB1 is coprecipitated with the mutants harboring the A/B domain (lanes 5 and 6; ΔA/P and A/B), suggesting that YB-1 interacts with vRNP through the A/B domain. Next, we tried to demonstrate whether YB-1 recruits vRNP on microtubules *in vitro*. Reconstituted microtubules were incubated with either vRNP or YB-1-vRNP complex and then subjected to immunoprecipitation using anti-NP antibody (Fig. 7C). We found that microtubules were hardly coprecipitated with vRNP in the absence of YB-1 (lane 4). In sharp contrast, in the presence of YB-1, the interaction of vRNP with microtubules was increased by approximately 3-fold (lane 5). Finally, we carried out immunoprecipitation assays with cell lysates prepared from cells constitutively expressing FLAG-α-tubulin with or without YB-1 KD (Fig. 7D). We found that PB1 was immunoprecipitated with FLAG-α-tubulin from control lysates (lane 3) but slightly from YB-1 KD lysates (lane 6). Therefore, it could be concluded that YB-1 is required for the accumulation of vRNP on microtubules. Taking these findings together, we propose that YB-1 interacts directly with vRNP and functions as a porter that facilitates the binding of vRNP with microtubules, where vRNP is led to Rab11a-positivie recycling endosomes.

DISCUSSION

We have identified YB-1, a cellular DNA/RNA-binding protein, as a vRNP-interacting protein (Fig. 1A). YB-1 was found to be relocalized to the nucleus from the cytoplasm and associated with PML NBs along with the progression of virus infection (Fig. 1B).

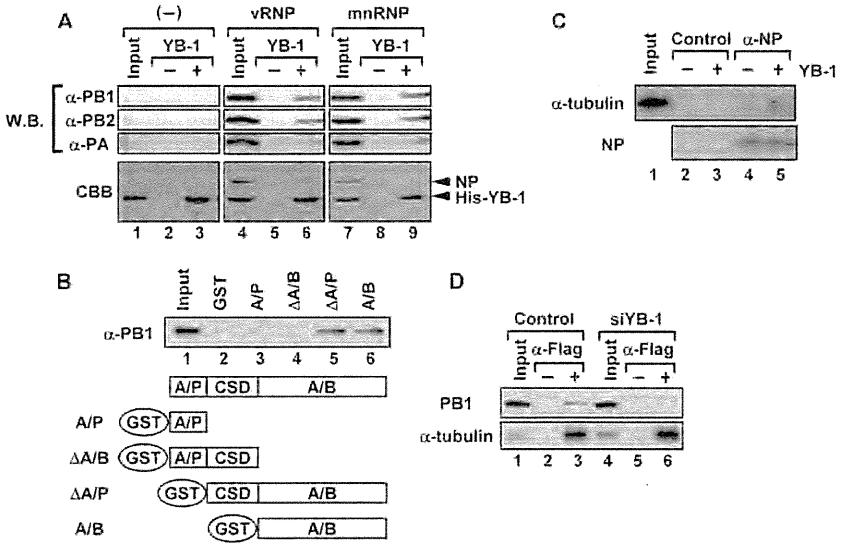

FIG 7 YB-1 functions as a porter bringing the progeny vRNP to microtubules. (A) Direct interaction of YB-1 with viral polymerase complex. vRNP (lanes 4 to 6) or micrococcal nuclease-treated vRNP (mnRNP) (lanes 7 to 9) was incubated in the absence (lanes 2, 5, and 8) or presence (lanes 3, 6, and 9) of purified recombinant His-YB-1 protein at 30°C for 1 h. Complexes were purified using Ni-NTA resin, and then proteins were separated through SDS-PAGE and detected by Coomassie brilliant blue (CBB) staining and Western blotting assays with anti-PB1, anti-PB2, and anti-PA antibodies. Lanes 1, 4, and 7 represent 20% of input amounts. (B) Interaction of vRNP with deletion mutants of YB-1. Each GST-fused deletion mutant of YB-1 was incubated with vRNP at 30°C for 1 h. Complexes were purified using glutathione-Sepharose resins, and then proteins were separated through SDS-PAGE and detected by Western blotting assays using anti-PB1 antibody. Lane 1 represents 20% of input amounts. A schematic diagram of the deletion mutants of YB-1 is at the bottom. (C) Interaction between vRNP and microtubules mediated by YB-1. Reconstituted microtubules were incubated with either vRNP (lanes 2 and 4) or YB-1-vRNP complex (lanes 3 and 5), and then complexes were immunoprecipitated with either a nonspecific IgG (control; lanes 2 and 3) or anti-NP antibody (lanes 4 and 5). The immunoprecipitated proteins were separated through SDS-PAGE and subjected to Western blotting assays with anti-α-tubulin and anti-NP antibodies. Lane 1 represents 10% of input amount. (D) Interaction of vRNP with microtubules in YB-1 KD cells. HeLa cells constitutively expressing FLAG-α-tubulin were infected with influenza virus at an MOI of 10. At 8 hpi, cell lysates were prepared and subjected to immunoprecipitation assays with either control IgG or anti-FLAG antibody. The immunoprecipitated proteins eluted with 100 μg/ml FLAG peptide were separated through SDS-PAGE and then visualized by Western blotting assays using anti-PB1 and anti-α-tubulin antibodies. Five percent equivalents of control (lane 1) and YB-1 KD (lane 4) lysates are also shown.

Previous reports showed that the nuclear import of YB-1 requires phosphorylation by protein kinase C (PKC) (35) and Jak1 (15) and Akt (69) kinases. The other mechanism for nuclear import of YB-1 is thought to be triggered by a proteolytic cleavage by 20S proteasomes to separate the C-terminal fragment (aa 220 to 324) containing a cytoplasmic retention signal (68). When we performed immunofluorescence assays with an antibody recognizing either the N terminus (aa 1 to 13) (used in this study) or the C terminus (aa 307 to 324) (purchased from Sigma), the YB-1 nuclear import was found only when the antibody recognizing the N terminus was used (data not shown). However, we found that vRNP complexes interact with full-length YB-1 (Fig. 1A), suggesting that the 20S proteasome-mediated processing of YB-1 may not always be required in influenza virus-infected cells. Therefore, it is possible that the recognition specificity of our antibody is due to an unknown conformational change of YB-1 possibly induced by the phosphorylation and/or interaction with cellular and/or viral proteins. Identification of a signaling pathway and interacting proteins responsible for the nuclear import of YB-1 upon influenza virus infection is needed.

PML NBs are highly dynamic structures that are disrupted or changed in their morphology in response to environmental stimuli (38). The genomes of several DNA viruses have been shown to be localized and transcribed in the vicinity of PML NBs (13, 23, 24). In most cases, virus-encoded regulatory proteins localize at PML NBs and disrupt PML NBs for successful infection, suggesting a negative role for PML NBs in virus growth (13, 23, 24). In addition to the putative function of PML NBs during virus infection, it is postulated that PML NBs have functions in cellular gene transcription, tumor suppression, proteasomal degradation, cellular senescence, apoptosis, and DNA repair (14, 38). It is proposed that PML NBs might modulate chromatin architecture and transcription, since nascent RNA and several gene loci are found around PML NBs (5, 13, 65). Given this, it seems likely that viruses hijack this nuclear structure to set up a platform suitable for virus replication, although the functional relevance of the interaction between influenza virus and PML NBs is an open question. M1 and NS2 were shown to be associated with PML NBs (62, 64), although the functional significance of the colocalization remains to be determined. We found that the YB-1 imported into the nucleus accumulates in PML NBs, in which vRNA was present with M1 and NS2 when the vRNP export was inhibited (Fig. 2). Therefore, we speculate that the progeny vRNPs could be assembled into the export complexes at PML NBs and subsequently interact with YB-1. Additional experiments are needed to clarify a precise role(s) of PML NBs in the vRNP nuclear export as well as the mechanism for targeting YB-1 to PML NBs.

The accumulation of recycling endosome vesicles around the MTOC is disrupted in the presence of microtubule depolymerization reagents such as nocodazole (8). Thus, it is likely that the intact microtubule functions as a platform for the recycling endosome vesicle. We observed a direct binding of YB-1 with vRNP for

the recruitment of vRNP to microtubules (Fig. 7). However, only a small portion of vRNP was colocalized with YB-1 in infected cells, suggesting that YB-1 transiently interacts with vRNP (Fig. 1). Further, we could not find YB-1 in the purified influenza virions (data not shown), suggesting that YB-1 might be dissociated from vRNP prior to packaging of vRNP into progeny virions. The association between YB-1 and enough microtubules is proposed to compete with the interaction of YB-1 with cellular mRNP *in vitro* (11). Thus, we speculate that vRNP-YB-1 complexes recruited on microtubules may be disassembled by the microtubule formation, and thereby vRNP could be loaded onto Rab11a-positive recycling endosomes bound to microtubules.

The Rab11a-mediated vesicular transport may be functionally important after arrival at the plasma membrane. For example, lipid rafts are required for the budding of influenza virus from the apical plasma membrane (63, 70), and cholesterol, an essential component of the lipid rafts, is enriched in the recycling endosome membrane (48). Interestingly, it has been shown that influenza virus particles are hardly pinched off from the plasma membrane in Rab11a KD cells (7). Thus, it is possible that the Rab11a-positive recycling endosome has an important role in the apical transport of proteins and/or membranes which are involved in budding process, including membrane scission (60). However, it is also possible that the trafficking of the viral genome is required to allow the efficient virus budding. The influenza virus genome consists of eight-segmented vRNA molecules. Since it is believed that the eight individual segments are packaged into a progeny virion (53), a hierarchical incorporation of each vRNA should be required. It is hypothesized that Rab11a-positive transport vesicles might be an assembly center of the eight segments of vRNA (17, 47). To further understand the mechanism of influenza virus egress, the dynamics of the recycling endocytic compartment are to be analyzed.

ACKNOWLEDGMENTS

We thank F. Momose (Kitasato University) for helpful discussion and K. Mizumoto (Kitasato University), K. Irie (University of Tsukuba), T. Naiki (University of Tsukuba), A. Kato (National Institute of Infectious Diseases, Japan), S. Hongo (Yamagata University), and K. Sugawara (Yamagata University) for generous gifts of purified tubulin proteins (K. Mizumoto), anti-TIAR antibody (K. Irie and T. Naiki), anti-SeV antibody (A. Kato), and mouse monoclonal anti-M1 antibody (S. Hongo and K. Sugawara). We also thank M. N. Asaka (University of Tsukuba) and T. Minowa (National Institute for Material Science) for their help with LC-MS analysis.

This research was supported in part by a grant-in-aid from the Ministry of Education, Culture, Sports, Science, and Technology of Japan (to K.N.) and Research Fellowships of the Japanese Society for the Promotion of Science (JSPS) (to A.K.).

REFERENCES

1. **Amorim MJ, et al.** 2011. A Rab11- and microtubule-dependent mechanism for cytoplasmic transport of influenza A virus viral RNA. J. Virol. 85:4143–4156.
2. **Anderson P, Kedersha N.** 2008. Stress granules: the Tao of RNA triage. Trends Biochem. Sci. 33:141–150.
3. **Anderson P, Kedersha N.** 2002. Stressful initiations. J. Cell Sci. 115:3227–3234.
4. **Bier K, York A, Fodor E.** 2011. Cellular cap-binding proteins associate with influenza virus mRNAs. J. Gen. Virol. 92:1627–1634.
5. **Boisvert FM, Hendzel MJ, Bazett-Jones DP.** 2000. Promyelocytic leukemia (PML) nuclear bodies are protein structures that do not accumulate RNA. J. Cell Biol. 148:283–292.
6. **Brock SC, Goldenring Jr, Crowe JE, Jr.** 2003. Apical recycling systems regulate directional budding of respiratory syncytial virus from polarized epithelial cells. Proc. Natl. Acad. Sci. U. S. A. 100:15143–15148.
7. **Bruce EA, Digard P, Stuart AD.** 2010. The Rab11 pathway is required for influenza A virus budding and filament formation. J. Virol. 84:5848–5859.
8. **Casanova JE, et al.** 1999. Association of Rab25 and Rab11a with the apical recycling system of polarized Madin-Darby canine kidney cells. Mol. Biol. Cell 10:47–61.
9. **Chambers R, Takimoto T.** 2010. Trafficking of Sendai virus nucleocapsids is mediated by intracellular vesicles. PLoS One 5:e10994. doi:10.1371/journal.pone.0010994.
10. **Chelbi-Alix MK, Quignon F, Pelicano L, Koken MH, de The H.** 1998. Resistance to virus infection conferred by the interferon-induced promyelocytic leukemia protein. J. Virol. 72:1043–1051.
11. **Chernov KG, et al.** 2008. Atomic force microscopy reveals binding of mRNA to microtubules mediated by two major mRNP proteins YB-1 and PABP. FEBS Lett. 582:2875–2881.
12. **Chernov KG, et al.** 2008. YB-1 promotes microtubule assembly in vitro through interaction with tubulin and microtubules. BMC Biochem. 9:23. doi:10.1186/1471-2091-9-23.
13. **Ching RW, Dellaire G, Eskiw CH, Bazett-Jones DP.** 2005. PML bodies: a meeting place for genomic loci? J. Cell Sci. 118:847–854.
14. **Dellaire G, Bazett-Jones DP.** 2004. PML nuclear bodies: dynamic sensors of DNA damage and cellular stress. Bioessays 26:963–977.
15. **Dooley S, et al.** 2006. Y-box protein-1 is the crucial mediator of antifibrotic interferon-gamma effects. J. Biol. Chem. 281:1784–1795.
16. **Dreyfuss G, Kim VN, Kataoka N.** 2002. Messenger-RNA-binding proteins and the messages they carry. Nat. Rev. Mol. Cell Biol. 3:195–205.
17. **Eisfeld AJ, Kawakami E, Watanabe T, Neumann G, Kawaoka Y.** 2011. RAB11A is essential for transport of the influenza virus genome to the plasma membrane. J. Virol. 85:6117–6126.
18. **Eliseeva IA, Kim ER, Guryanov SG, Ovchinnikov LP, Lyabin DN.** 2011. Y-box-binding protein 1 (YB-1) and its functions. Biochemistry (Mosc.) 76:1402–1433.
19. **Elton D, et al.** 2001. Interaction of the influenza virus nucleoprotein with the cellular CRM1-mediated nuclear export pathway. J. Virol. 75:408–419.
20. **Engelhardt OG, Sirma H, Pandolfi PP, Haller O.** 2004. Mx1 GTPase accumulates in distinct nuclear domains and inhibits influenza A virus in cells that lack promyelocytic leukaemia protein nuclear bodies. J. Gen. Virol. 85:2315–2326.
21. **Eulalio A, Behm-Ansmant I, Izaurralde E.** 2007. P bodies: at the crossroads of post-transcriptional pathways. Nat. Rev. Mol. Cell Biol. 8:9–22.
22. **Evdokimova V, et al.** 2001. The major mRNA-associated protein YB-1 is a potent 5′ cap-dependent mRNA stabilizer. EMBO J. 20:5491–5502.
23. **Everett RD.** 2006. Interactions between DNA viruses, ND10 and the DNA damage response. Cell. Microbiol. 8:365–374.
24. **Everett RD, Chelbi-Alix MK.** 2007. PML and PML nuclear bodies: implications in antiviral defence. Biochimie 89:819–830.
25. **Grant BD, Donaldson JG.** 2009. Pathways and mechanisms of endocytic recycling. Nat. Rev. Mol. Cell Biol. 10:597–608.
26. **Herz C, Stavnezer E, Krug R, Gurney T.** 1981. Influenza virus, an RNA virus, synthesizes its messenger RNA in the nucleus of infected cells. Cell 26:391–400.
27. **Iki S, et al.** 2005. Serum-dependent expression of promyelocytic leukemia protein suppresses propagation of influenza virus. Virology 343:106–115.
28. **Jo S, et al.** 2010. Involvement of vesicular trafficking system in membrane targeting of the progeny influenza virus genome. Microbes Infect. 12:1079–1084.
29. **Jorba N, et al.** 2008. Analysis of the interaction of influenza virus polymerase complex with human cell factors. Proteomics 8:2077–2088.
30. **Kawaguchi A, Momose F, Nagata K.** 2011. Replication-coupled and host factor-mediated encapsidation of the influenza virus genome by viral nucleoprotein. J. Virol. 85:6197–6204.
31. **Kawaguchi A, Naito T, Nagata K.** 2005. Involvement of influenza virus PA subunit in assembly of functional RNA polymerase complexes. J. Virol. 79:732–744.
32. **Kawakami K, Ishihama A.** 1983. RNA polymerase of influenza virus. III. Isolation of RNA polymerase-RNA complexes from influenza virus PR8. J. Biochem. 93:989–996.

33. **Keene JD.** 2010. Global regulation and dynamics of ribonucleic acid. Endocrinology **151**:1391–1397.
34. **Kohno K, Izumi H, Uchiumi T, Ashizuka M, Kuwano M.** 2003. The pleiotropic functions of the Y-box-binding protein, YB-1. Bioessays **25**: 691–698.
35. **Koike K, et al.** 1997. Nuclear translocation of the Y-box binding protein by ultraviolet irradiation. FEBS Lett. **417**:390–394.
36. **Krzyzaniak MA, Mach M, Britt WJ.** 2009. HCMV-encoded glycoprotein M (UL100) interacts with Rab11 effector protein FIP4. Traffic **10**:1439–1457.
37. **Kuwano M, et al.** 2003. The basic and clinical implications of ABC transporters, Y-box-binding protein-1 (YB-1) and angiogenesis-related factors in human malignancies. Cancer Sci. **94**:9–14.
38. **Lallemand-Breitenbach V, de The H.** 2010. PML nuclear bodies. Cold Spring Harbor Perspect. Biol. **2**:a000661. doi:10.1101/cshperspect.a000661.
39. **Martin K, Helenius A.** 1991. Nuclear transport of influenza virus ribonucleoproteins: the viral matrix protein (M1) promotes export and inhibits import. Cell **67**:117–130.
40. **Matsumoto K, et al.** PRMT1 is required for RAP55 to localize to processing bodies. RNA Biol. **9**:610–623.
41. **Matsumoto K, Wolffe AP.** 1998. Gene regulation by Y-box proteins: coupling control of transcription and translation. Trends Cell Biol. **8**:318–323.
42. **Maxfield FR, McGraw TE.** 2004. Endocytic recycling. Nat. Rev. Mol. Cell Biol. **5**:121–132.
43. **Mayer D, et al.** 2007. Identification of cellular interaction partners of the influenza virus ribonucleoprotein complex and polymerase complex using proteomic-based approaches. J. Proteome Res. **6**:672–682.
44. **Momose F, et al.** 2001. Cellular splicing factor RAF-2p48/NPI-5/BAT1/UAP56 interacts with the influenza virus nucleoprotein and enhances viral RNA synthesis. J. Virol. **75**:1899–1908.
45. **Momose F, Kikuchi Y, Komase K, Morikawa Y.** 2007. Visualization of microtubule-mediated transport of influenza viral progeny ribonucleoprotein. Microbes Infect. **9**:1422–1433.
46. **Momose F, et al.** 2002. Identification of Hsp90 as a stimulatory host factor involved in influenza virus RNA synthesis. J. Biol. Chem. **277**:45306–45314.
47. **Momose F, et al.** 2011. Apical transport of influenza A virus ribonucleoprotein requires Rab11-positive recycling endosome. PLoS One **6**:e21123. doi:10.1371/journal.pone.0021123.
48. **Mukherjee S, Zha X, Tabas I, Maxfield FR.** 1998. Cholesterol distribution in living cells: fluorescence imaging using dehydroergosterol as a fluorescent cholesterol analog. Biophys. J. **75**:1915–1925.
49. **Nagata K, Kawaguchi A, Naito T.** 2008. Host factors for replication and transcription of the influenza virus genome. Rev. Med. Virol. **18**:247–260.
50. **Naito T, Momose F, Kawaguchi A, Nagata K.** 2007. Involvement of Hsp90 in assembly and nuclear import of influenza virus RNA polymerase subunits. J. Virol. **81**:1339–1349.
51. **Nayak DP, Hui EK, Barman S.** 2004. Assembly and budding of influenza virus. Virus Res. **106**:147–165.
52. **Neumann G, Hughes MT, Kawaoka Y.** 2000. Influenza A virus NS2 protein mediates vRNP nuclear export through NES-independent interaction with hCRM1. EMBO J. **19**:6751–6758.
53. **Noda T, et al.** 2006. Architecture of ribonucleoprotein complexes in influenza A virus particles. Nature **439**:490–492.
54. **O'Neill RE, Talon J, Palese P.** 1998. The influenza virus NEP (NS2 protein) mediates the nuclear export of viral ribonucleoproteins. EMBO J. **17**:288–296.
55. **Pisarev AV, et al.** 2002. Positive and negative effects of the major mammalian messenger ribonucleoprotein p50 on binding of 40 S ribosomal subunits to the initiation codon of beta-globin mRNA. J. Biol. Chem. **277**:15445–15451.
56. **Portela A, Digard P.** 2002. The influenza virus nucleoprotein: a multifunctional RNA-binding protein pivotal to virus replication. J. Gen. Virol. **83**:723–734.
57. **Read EK, Digard P.** 2010. Individual influenza A virus mRNAs show differential dependence on cellular NXF1/TAP for their nuclear export. J. Gen. Virol. **91**:1290–1301.
58. **Rees PJ, Dimmock NJ.** 1981. Electrophoretic separation of influenza virus ribonucleoproteins. J. Gen. Virol. **53**:125–132.
59. **Robb NC, et al.** 2011. The influenza A virus NS1 protein interacts with the nucleoprotein of viral ribonucleoprotein complexes. J. Virol. **85**:5228–5231.
60. **Rossman JS, Jing X, Leser GP, Lamb RA.** 2010. Influenza virus M2 protein mediates ESCRT-independent membrane scission. Cell **142**:902–913.
61. **Rowe RK, Suszko JW, Pekosz A.** 2008. Roles for the recycling endosome, Rab8, and Rab11 in hantavirus release from epithelial cells. Virology **382**: 239–249.
62. **Sato Y, et al.** 2003. Localization of influenza virus proteins to nuclear dot 10 structures in influenza virus-infected cells. Virology **310**:29–40.
63. **Scheiffele P, Rietveld A, Wilk T, Simons K.** 1999. Influenza viruses select ordered lipid domains during budding from the plasma membrane. J. Biol. Chem. **274**:2038–2044.
64. **Shibata T, Tanaka T, Shimizu K, Hayakawa S, Kuroda K.** 2009. Immunofluorescence imaging of the influenza virus M1 protein is dependent on the fixation method. J. Virol. Methods **156**:162–165.
65. **Shiels C, et al.** 2001. PML bodies associate specifically with the MHC gene cluster in interphase nuclei. J. Cell Sci. **114**:3705–3716.
66. **Shimizu K, Handa H, Nakada S, Nagata K.** 1994. Regulation of influenza virus RNA polymerase activity by cellular and viral factors. Nucleic Acids Res. **22**:5047–5053.
67. **Sloboda RD, Dentler WL, Rosenbaum JL.** 1976. Microtubule-associated proteins and the stimulation of tubulin assembly in vitro. Biochemistry **15**:4497–4505.
68. **Sorokin AV, et al.** 2005. Proteasome-mediated cleavage of the Y-box-binding protein 1 is linked to DNA-damage stress response. EMBO J. **24**:3602–3612.
69. **Sutherland BW, et al.** 2005. Akt phosphorylates the Y-box binding protein 1 at Ser102 located in the cold shock domain and affects the anchorage-independent growth of breast cancer cells. Oncogene **24**:4281–4292.
70. **Takeda M, Leser GP, Russell CJ, Lamb RA.** 2003. Influenza virus hemagglutinin concentrates in lipid raft microdomains for efficient viral fusion. Proc. Natl. Acad. Sci. U. S. A. **100**:14610–14617.
71. **Tanaka KJ, et al.** 2006. RAP55, a cytoplasmic mRNP component, represses translation in Xenopus oocytes. J. Biol. Chem. **281**:40096–40106.
72. **Tay WL, et al.** 2009. Y-Box-binding protein-1 is a promising predictive marker of radioresistance and chemoradioresistance in nasopharyngeal cancer. Mod. Pathol. **22**:282–290.
73. **Utley TJ, et al.** 2008. Respiratory syncytial virus uses a Vps4-independent budding mechanism controlled by Rab11-FIP2. Proc. Natl. Acad. Sci. U. S. A. **105**:10209–10214.
74. **van Ijzendoorn SC.** 2006. Recycling endosomes. J. Cell Sci. **119**:1679–1681.
75. **Wakabayashi Y, Dutt P, Lippincott-Schwartz J, Arias IM.** 2005. Rab11a and myosin Vb are required for bile canalicular formation in WIF-B9 cells. Proc. Natl. Acad. Sci. U. S. A. **102**:15087–15092.
76. **Watanabe K, et al.** 2006. Identification of Hsc70 as an influenza virus matrix protein (M1) binding factor involved in the virus life cycle. FEBS Lett. **580**:5785–5790.
77. **Watanabe K, et al.** 2001. Inhibition of nuclear export of ribonucleoprotein complexes of influenza virus by leptomycin B. Virus Res. **77**:31–42.
78. **Yang WH, Bloch DB.** 2007. Probing the mRNA processing body using protein macroarrays and "autoantigenomics." RNA **13**:704–712.
79. **Zhang J, Pekosz A, Lamb RA.** 2000. Influenza virus assembly and lipid raft microdomains: a role for the cytoplasmic tails of the spike glycoproteins. J. Virol. **74**:4634–4644.

JVI
Journals.ASM.org

Replication-Uncoupled Histone Deposition during Adenovirus DNA Replication

Tetsuro Komatsu and Kyosuke Nagata

Department of Infection Biology, Faculty of Medicine and Graduate School of Comprehensive Human Sciences, University of Tsukuba, Tsukuba, Japan

In infected cells, the chromatin structure of the adenovirus genome DNA plays critical roles in its genome functions. Previously, we reported that in early phases of infection, incoming viral DNA is associated with both viral core protein VII and cellular histones. Here we show that in late phases of infection, newly synthesized viral DNA is also associated with histones. We also found that the knockdown of CAF-1, a histone chaperone that functions in the replication-coupled deposition of histones, does not affect the level of histone H3 bound on viral chromatin, although CAF-1 is accumulated at viral DNA replication foci together with PCNA. Chromatin immunoprecipitation assays using epitope-tagged histone H3 demonstrated that histone variant H3.3, which is deposited onto the cellular genome in a replication-independent manner, is selectively associated with both incoming and newly synthesized viral DNAs. Microscopic analyses indicated that histones but not USF1, a transcription factor that regulates viral late gene expression, are excluded from viral DNA replication foci and that this is achieved by the oligomerization of the DNA binding protein (DBP). Taken together, these results suggest that histone deposition onto newly synthesized viral DNA is most likely uncoupled with viral DNA replication, and a possible role of DBP oligomerization in this replication-uncoupled histone deposition is discussed.

In the cell nucleus, the genomic DNA is not naked but forms a chromatin structure with chromatin proteins. The fundamental unit of the chromatin structure is the nucleosome, which consists of a histone octamer (two copies each of histones H2A, H2B, H3, and H4) and DNA wrapping around the octamer. The deposition of histones and/or the remodeling of nucleosome arrays is a critical process for the expression of genome functions (2), since nucleosome packaging could be a barrier for *trans*-acting factors to access their cognate sites on DNA. Thus, the nucleosome structure must be strictly and dynamically regulated in connection with several events on chromatin, such as transcription, DNA replication, and DNA repair.

Currently, it is known that histone deposition is carried out mainly in two fashions, DNA replication-dependent and independent ones, and a role of histone variants in these deposition pathways has been elucidated (14). In mammalian somatic cells, there are three major histone H3 variants, H3.1, H3.2, and H3.3, and they have only slight differences in amino acid sequences (16). The canonical histone H3, histone H3.1, and the highly related variant H3.2 (which differs by only 1 amino acid [aa] from H3.1) are expressed exclusively during the S phase, while the expression of the variant H3.3, which differs by 4 and 5 aa from H3.2 and H3.1, respectively, is observed throughout the cell cycle. Thus, this variant is called a "replication-independent" one (11). Tagami et al. demonstrated previously that the canonical histone H3 (H3.1) interacts with the histone chaperone CAF-1 complex and is deposited onto DNA in a replication-dependent manner, while HIRA specifically binds to and deposits histone variant H3.3 onto DNA independently of DNA synthesis (43). CAF-1 is composed of three subunits, p150, p60, and p48, and is associated with the cellular DNA replication machinery through an interaction with PCNA, a sliding clamp for DNA polymerases, allowing the DNA replication-coupled deposition of histones (40, 41, 50). On the other hand, HIRA was identified as a DNA synthesis-independent histone chaperone in cell-free systems using *Xenopus laevis* egg extracts (32), and histone variant H3.3 was shown to mark transcriptionally active genomic regions (1). Furthermore, additional H3.3-specific chaperones were recently identified. Daxx is one of the components of promyelocytic leukemia (PML) nuclear bodies and was reported to deposit histone H3.3 onto specific genomic regions, such as telomeres and pericentric heterochromatin, together with an ATP-dependent chromatin remodeler, ATRX (10, 21). It was also reported that in *Drosophila melanogaster* cells, DEK is a coactivator of a nuclear receptor and functions as an H3.3-specific chaperone (37). Thus, the mechanistic evidences for histone deposition are accumulating in the case of cellular chromatin.

The regulatory events for the chromatin structure are not limited to the cellular genome, as some viruses also have chromatin and/or chromatin-like structures with their own genomes. The adenovirus (Ad) genome is a linear double-stranded DNA (dsDNA) of ~36,000 bp in length. In the virion, the Ad genome forms a chromatin-like structure with viral basic core proteins, as revealed by electron microscopic analyses showing that viral core protein-DNA complexes purified from the virion show a "beads-on-a-string" structure (49). Among core proteins, protein VII is a major DNA binding protein that can introduce superhelical turns into DNA, as do cellular histones (4), and remains associated with viral DNA after nuclear import of the virus genome (7, 17). When viral DNA-core protein complexes purified from the virion are used as a template for cell-free DNA replication/transcription systems, the reactions occur at a much lower level than in the case of naked DNA, indicating that the viral chromatin-like structure must be remodeled to execute its genome functions (22, 23). Pre-

Received 14 February 2012 Accepted 3 April 2012
Published ahead of print 11 April 2012
Address correspondence to Kyosuke Nagata, knagata@md.tsukuba.ac.jp.

doi:10.1128/JVI.00380-12

viously, we identified host cell-derived remodeling factors for Ad chromatin by biochemical analyses (19, 22, 24, 26) and demonstrated that TAF-I, one of these host factors, plays an important role in the regulation of viral early gene expression in infected cells through interactions with protein VII (15, 17, 18, 20, 27). Thus, it was indicated that the remodeling of Ad chromatin is a crucial process for its genome functions (13), as is the case for the cellular genome. In addition, using chromatin immunoprecipitation (ChIP) assays, we recently reported that in early phases of infection, cellular histones are incorporated into viral DNA-protein VII complexes and that a histone modification occurs depending upon the transcription states on viral chromatin, suggesting that cellular histones could be functional components of viral chromatin in infected cells (20).

As described above, although the viral chromatin structure and its regulation in early phases of infection are being clarified, it is quite unclear how the viral chromatin structure is regulated in late phases of infection. In particular, since the expression of viral late genes is dependent largely on its own DNA replication (45), the regulation of the chromatin structure during viral DNA replication could be a key step. Therefore, in this study, we sought to elucidate the regulatory mechanism of how the chromatin structure is formed on newly synthesized viral DNA through viral DNA replication, in particular with respect to histone deposition. We found that after the onset of viral DNA replication, cellular histones are also incorporated into viral chromatin. We also found that although CAF-1 is accumulated at the site of viral DNA replication, this factor seems not to be involved in histone deposition during viral DNA replication, since the knockdown of CAF-1 did not affect the binding level of histone H3 on viral chromatin, and that histone variant H3.3, which is deposited onto DNA in a DNA synthesis-independent manner, is specifically deposited onto viral DNA even after the onset of viral DNA replication. Microscopic analyses suggested that histones but not USF1, a transcription factor which was shown previously to bind to and regulate transcription from the viral major late promoter (MLP) (46), are excluded form the site of viral DNA replication, possibly by the oligomerization of Ad single-stranded DNA (ssDNA) binding protein (DBP), one of the viral DNA replication factors. Based on these results, we propose a model whereby, unlike cellular chromatin, histone deposition onto the newly synthesized viral DNA is not coupled with viral DNA replication. A feasible role of this uncoupled deposition mechanism mediated by DBP oligomerization in Ad genome functions is discussed.

MATERIALS AND METHODS

Cells and viruses. The maintenance of HeLa cells and the purification and infection of human adenovirus type 5 (HAdV5) were carried out essentially as described previously (18, 20). Hydroxyurea (HU) was added at a final concentration of 2 mM immediately after infection when DNA replication was to be blocked. HeLa cells stably expressing enhanced green fluorescent protein (EGFP)-tagged histones H3.2 and H3.3 (a kind gift from M. Okuwaki, University of Tsukuba) were also maintained as described above. The transfection of expression plasmids was performed by using GeneJuice (Novagen) according to the manufacturer's protocol.

Antibodies. Antibodies used in this study are as follows: rabbit anti-histone H3 (catalog no. ab1791; Abcam), rabbit anti-histone H4 (catalog no. 04-858; Millipore), rabbit anti-histone H2A (catalog no. ab18255; Abcam), mouse anti-HIRA (catalog no. 04-1488; Millipore), mouse anti-FLAG M2 (catalog no. F3165; Sigma), rat anti-hemagglutinin (HA) (3F10; Roche), and mouse anti-β-actin (Sigma) antibodies. Rabbit anti-histone H2A-H2B, mouse anti-CAF-1 p150, and mouse anti-DBP antibodies were kindly provided by M. Okuwaki (University of Tsukuba), A. Verreault (University of Montreal), and W. C. Russel, respectively. Rat anti-protein VII antibody was described elsewhere previously (17).

Vector construction. To construct the expression vectors for USF1, full-length DBP, and its deletion mutant (DBPΔC, which lacks the C-terminal 17 aa), cDNA fragments of USF1, DBP, and DBPΔC were amplified by PCR; digested with BamHI and EcoRI; and cloned in frame into the pCHA vector containing an HA epitope tag and the puromycin resistance gene (pCHA-puro vector; kindly provided by K. Kajitani, University of Tsukuba). The resulting vectors were designated pCHA-puro-USF1, pCHA-puro-DBP, and pCHA-puro-DBPΔC, respectively. Similarly, for the expression vector of PCNA, an amplified cDNA fragment was digested with BamHI and cloned into the pCHA-puro vector digested with BamHI and EcoRV (pCHA-puro-PCNA). The primers used here were as follows: 5′-GTTTAGGATCCCATATGAAGGGGCAGCAG-3′ and 5′-GGGCCG AATTCTTAGTTGCTGTCATTCTTG-3′ for USF1 cDNA, 5′-AAAGGA TCCATGGCCAGTCGGG-3′ and 5′-GCGGAATTCTTAAAAATCAAA GGGGTTCTG-3′ for DBP cDNA, 5′-AAAGGATCCATGGCCAGTCGG G-3′ and 5′-CCCGAATTCTTAGTTGCGATACTGG-3′ for DBPΔC cDNA, and 5′-AAAGGATCCATGTTCGAGGCGC-3′ and 5′-ATCGTC GACCTAAGATCCTTCTTC-3′ for PCNA cDNA.

For the preparation of cells stably expressing HA-PCNA, HeLa cells were transfected with pCHA-puro-PCNA and cultured in the presence of 2 μg/ml puromycin for 2 weeks.

For the construction of the expression vector of histone H3.1, a cDNA fragment of histone H3.1 was amplified by PCR, digested with NcoI, and cloned into the pBS-FLAG vector (pBS-H3.1-FLAG). The DNA fragment containing cDNA of H3.1 and the C-terminal FLAG tag was then obtained from pBS-H3.1-FLAG by digestion with BamHI and EcoRI and cloned into the pcDNA3 vector (pcDNA3-H3.1-FLAG). The primers used here were as follows: 5′-AAAACCATGGCGCGTACTAAGCAG-3′ and 5′-TT ATTCCATGGCCGCCCTCTCCCCA-3′.

The expression vectors for FLAG-tagged histones H3.2 and H3.3 (pcDNA3-H3.2-FLAG and pcDNA3-H3.3-FLAG, respectively) and HA-tagged DEK (pCHA-DEK) were generously provided by M. Okuwaki and S. Saito, respectively (University of Tsukuba).

Indirect immunofluorescence assays. Indirect immunofluorescence (IF) assays were carried out essentially as previously described (18). The localization of the protein was visualized with secondary antibodies (anti-mouse IgG conjugated with Alexa Fluor 488, anti-mouse IgG conjugated with Alexa Fluor 568, and anti-rabbit IgG conjugated with Alexa Fluor 568; Invitrogen). DNA was visualized by staining with TO-PRO-3 iodide (Invitrogen). Labeled cells were observed by confocal laser scanning microscopy (LSM5 Exciter; Carl Zeiss), using argon laser (488 nm) and He/Ne laser (546 and 633 mm) lines.

ChIP, RT-PCR, siRNA-mediated knockdown, and Western blot assays. ChIP, reverse transcription (RT)-PCR, small interfering RNA (siRNA)-mediated knockdown, and Western blot assays were carried out essentially as described previously (20). siRNA targeted for CAF-1 p150 was purchased commercially (Stealth siRNA; Invitrogen). Primers used for CAF-1 p150 mRNA are as follows: 5′-GGAGCAGGACAGTTGGAGT G-3′ and 5′-GACGAATGGCTGAGTACAGA-3′. Other primers for ChIP and RT-PCR assays were described elsewhere previously (20). In ChIP and RT-PCR assays using quantitative PCR (qPCR), the obtained cDNAs were quantitatively measured by qPCR, and mean values with standard deviations (SD) were obtained from three independent experiments.

RESULTS

Cellular histones are bound with viral chromatin in both early and late phases of infection. Previously, we reported that in early phases of infection (before the onset of viral DNA replication), viral chromatin is composed of both viral core protein VII and cellular histones and that this "chimeric" chromatin functions as the template for transcription (20). To examine whether histones

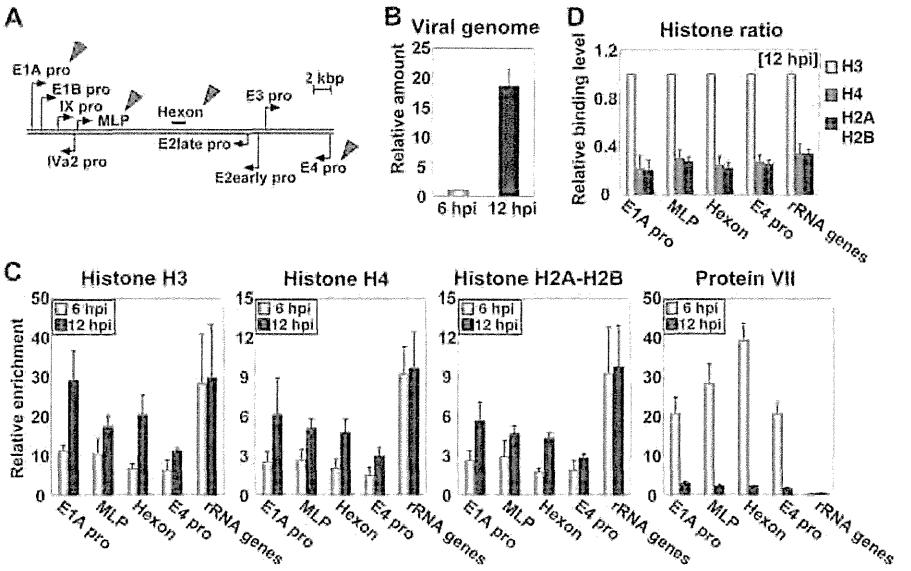

FIG 1 Viral chromatin structure in early and late phases of infection. (A) Structure of the Ad genome. Arrows represent promoters of viral genes. Target regions for ChIP assays are indicated by arrowheads. (B) Amounts of viral DNA. HeLa cells were infected with HAdV5 at an MOI of 100, and DNA samples were purified from infected cells at 6 and 12 hpi. The amount of viral DNA was quantitatively measured by qPCR using primers for the E1A promoter region. The amount of viral DNA is graphed as a ratio relative to that at 6 hpi. (C) ChIP assays. HeLa cells were infected with HAdV5 at an MOI of 100 and subjected to ChIP assays using infected cells at 6 and 12 hpi. Immunoprecipitation was carried out by using the indicated antibodies and an anti-FLAG antibody (as a negative control). The obtained DNAs were quantitatively measured by qPCR using the indicated primer sets. The binding levels of each protein were calculated as relative enrichment against that obtained in a negative control (anti-FLAG antibody). (D) Binding levels of core histones. Based on the results of ChIP assays, shown in panel C, the binding levels of histone H4 and H2A-H2B were normalized to that of histone H3.

are also bound with viral chromatin after the onset of viral DNA replication, we performed ChIP assays using antibodies against histones and protein VII (Fig. 1). Viral DNA replication starts at around 8 hpi (hours postinfection) under our conditions (17, 20). In order to reveal the viral chromatin state during or immediately after viral DNA replication, HeLa cells infected at an MOI (multiplicity of infection) of 100 were harvested at 6 and 12 hpi for ChIP assays. We chose five regions for ChIP assays, four viral genome regions (E1A pro, MLP, hexon, and E4 pro) (Fig. 1A) and one cellular genomic region (rRNA gene) as a control (20). Under this condition, the amount of viral DNA was increased by ~20-fold through viral DNA replication (Fig. 1B). At 6 hpi, all core histones were bound with viral chromatin but at a low binding level compared with that of cellular chromatin (histones H3, H4, and H2A-H2B) (Fig. 1C). This was in good agreement with our previous observations (20). At 12 hpi, core histones were also found to be associated with viral chromatin. The binding level of histones on viral chromatin at 12 hpi was higher than that at 6 hpi but slightly lower than that on cellular chromatin. This is consistent with a previous report of electron microscopic analyses showing that viral genome DNA purified from infected cells at late phases of infection has nucleosome-like particles, which are less dense than those in cellular nucleosome arrays (3). In contrast, the binding level of protein VII was drastically decreased after the onset of viral DNA replication (Fig. 1C), suggesting that newly synthesized viral DNA is associated mainly with cellular histones. We do not exclude the possibility that protein VII remains associated with a small population of viral chromatin, because the binding level of protein VII on viral chromatin was still higher than that on cellular chromatin even at 12 hpi. The ratio among core histones bound on viral chromatin was almost the same as that among core histones bound on cellular chromatin both at 6 hpi (20; data not shown) and at 12 hpi (Fig. 1D), indicating that viral chromatin contains the canonical nucleosome structure.

CAF-1 and PCNA are not involved in histone deposition onto newly synthesized viral DNA. It is known that during the DNA replication of the cellular genome and some DNA virus genomes, histones are deposited by CAF-1, a replication-dependent histone chaperone (41, 43). CAF-1 is associated with the DNA replication machinery through interactions with PCNA, thereby enabling the replication-coupled deposition of histone H3-H4 complexes (40). Thus, it was worthwhile to examine whether CAF-1 and PCNA are also involved in the histone deposition onto newly synthesized Ad DNA, although there is no definitive evidence that these two are involved in Ad DNA replication. To test this, we first performed IF assays using cells stably expressing HA-tagged PCNA (HA-PCNA) to examine the relationship among viral DNA replication, PCNA, and CAF-1 (Fig. 2A). By using an antibody against DBP, an Ad ssDNA binding protein involved in viral DNA replication, the places for viral DNA replication, designated "viral DNA replication foci" (here referred to as "VDRF"), can be visualized (31). HeLa cells or cells stably expressing HA-PCNA were infected at an MOI of 50, and at 18 hpi, the cells were subjected to IF assays using anti-DBP and anti-HA antibodies. In mock-infected cells, HA-PCNA was localized throughout the nucleus and showed a punctate localization in some cell populations, as reported previously (29). At 18 hpi, VDRF was observed as a donut-like signal by using an anti-DBP antibody, and we found that HA-PCNA, showing a punctate localization, was accumulated inside VDRF. We also observed a similar localization pattern

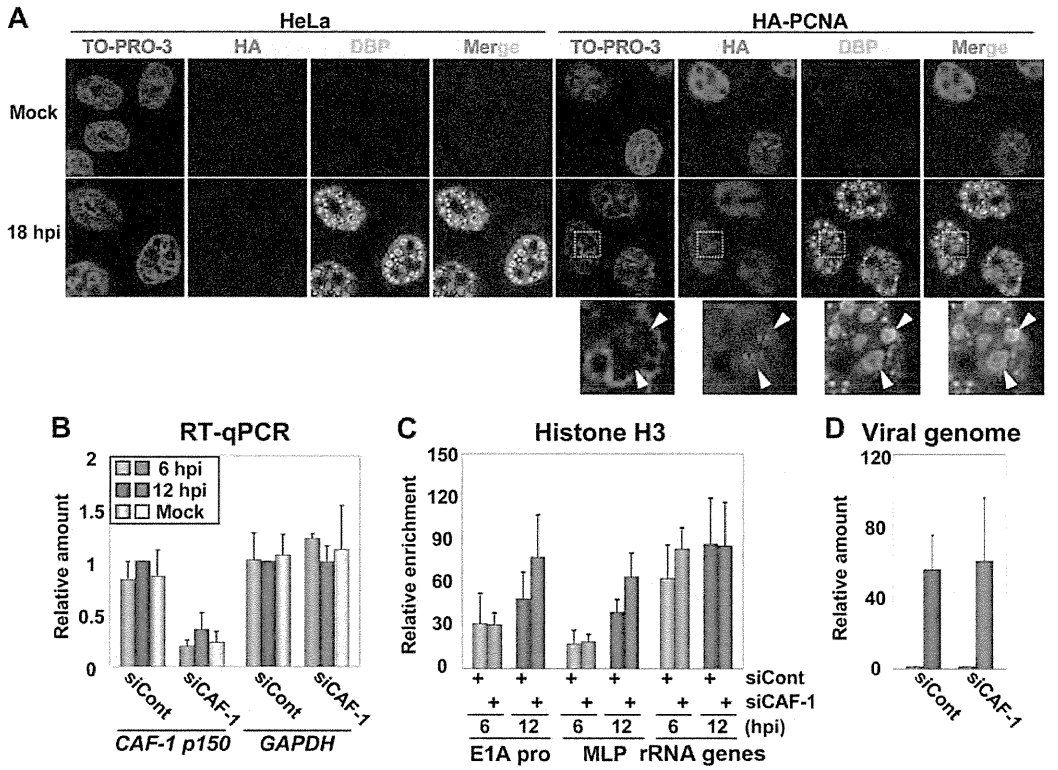

FIG 2 Localization and role of PCNA and CAF-1 during viral DNA replication. (A) IF assays. HeLa cells and cells stably expressing HA-PCNA grown on coverslips were mock infected or infected with HAdV5 at an MOI of 50. At 18 hpi, the localization patterns of HA-PCNA and DBP were analyzed by IF using anti-HA and anti-DBP antibodies. DNA was visualized by TO-PRO-3 iodide staining. Merged images are also indicated. Higher-magnification images of the regions marked by squares are shown below. (B) RT-qPCR assays. HeLa cells were treated with siCont or siCAF-1 and then either mock infected or infected with HAdV5 at an MOI of 100, and total RNAs were purified at 6 and 12 hpi. cDNAs were synthesized with reverse transcription and subjected to qPCR using primer sets for CAF-1 p150 and GAPDH mRNAs. The mRNA levels relative to those of control cells at 12 hpi were graphed. (C) ChIP assays. siRNA-treated cells were infected with HAdV5 at an MOI of 100, and at 6 and 12 hpi, the cells were subjected to ChIP assays using anti-histone H3 and anti-FLAG antibodies. (D) Relative amounts of viral DNA. Viral DNA was purified from lysates for ChIP assays (C) and subjected to qPCR using the primer set for the E1A promoter. The DNA amounts at 12 hpi relative to those at 6 hpi are shown.

of CAF-1 inside VDRF (see Fig. 4A). These results suggest that PCNA and CAF-1 are recruited together to the site of viral DNA replication.

Next, to investigate a role of CAF-1 in histone deposition onto viral DNA, the siRNA-mediated knockdown of CAF-1 p150, the largest subunit of the CAF-1 complex, was carried out (Fig. 2B to D). HeLa cells were treated with control siRNA (siCont) or siRNA for CAF-1 p150 (siCAF-1), infected with HAdV5 at an MOI of 100, and harvested at 6 and 12 hpi. First, we examined the knockdown efficiency of CAF-1 p150 by RT-qPCR assays (Fig. 2B). The mRNA level of CAF-1 p150 in siRNA-treated cells was about 20% of that in control cells, although at 12 hpi, the level was slightly increased, possibly due to the S-phase-like environment induced by Ad infection (30). In contrast, the mRNA level of glyceraldehyde-3-phosphate dehydrogenase (GAPDH) was almost unaffected by siRNA treatment and Ad infection. Under this condition, the binding level of histone H3 on viral chromatin was examined by ChIP assays (Fig. 2C). The binding level of H3 on viral chromatin was not decreased by the CAF-1 knockdown and, rather, slightly increased (but not statistically significantly) at 12 hpi (E1A pro and MLP) (Fig. 2C). Note that the binding level of H3 on cellular chromatin was also unaffected by the CAF-1 knockdown (rRNA gene) (Fig. 2C, and see Discussion). In addition, we could not observe any effect of the CAF-1 knockdown on viral DNA replication levels (Fig. 2D). Taken together, these results suggest that it is not likely that CAF-1 is involved in the histone deposition onto viral chromatin during viral DNA replication, although CAF-1 was accumulated at VDRF together with PCNA.

Replication-independent histone H3.3 is selectively incorporated into viral chromatin. It is known that among histone H3 variants, histones H3.1 and H3.2 are deposited onto DNA by CAF-1 during DNA replication, while H3.3 is deposited independently of DNA replication (11, 14). If CAF-1 is not involved in histone deposition during viral DNA replication, histone H3.3, rather than H3.1 and H3.2, could be incorporated into newly synthesized viral DNA. Therefore, to examine this possibility, we performed ChIP assays using FLAG-tagged histones H3.2 and H3.3 (Fig. 3). HeLa cells were transfected with expression vectors for H3.2 and H3.3, and at 24 hpt (hours posttransfection), the cells were infected at an MOI of 100. We first studied cells at early phases of infection (before the onset of viral DNA replication) (Fig. 3A). Infected cells were harvested at 2 and 6 hpi as well as at 10 hpi in the presence of HU to block viral DNA replication (20)

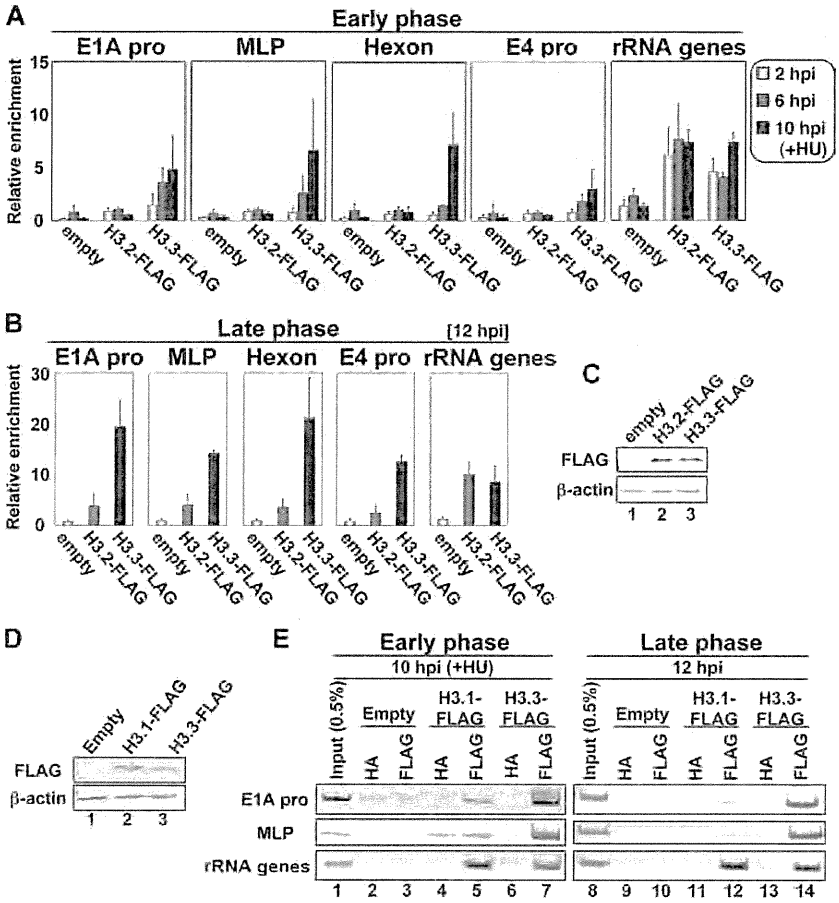

FIG 3 Incorporation of histone H3 variants into viral chromatin. (A and B) ChIP assays with FLAG-tagged histone H3 variants. HeLa cells were transfected with the pcDNA3 empty vector, pcDNA3-H3.2-FLAG, or pcDNA3-H3.3-FLAG and infected with HAdV5 at an MOI of 100 at 24 hpt (hours posttransfection). At 2, 6, and 10 hpi (A) or at 12 hpi (B), ChIP assays were carried out by using anti-FLAG and anti-HA (as a negative control) antibodies. Note that at 10 hpi, HU was added to block viral DNA replication. The results were graphed as relative enrichments. (C) Western blot analyses. At 24 hpt, lysates were prepared from cells transfected with the pcDNA3 empty vector (lane 1), pcDNA3-H3.2-FLAG (lane 2), and pcDNA3-H3.3-FLAG (lane 3) and subjected to 15% SDS-PAGE, followed by Western blot analyses using anti-FLAG (top) and anti-β-actin (bottom) antibodies. (D) Western blot analyses. HeLa cells were transfected with the pcDNA3 empty vector (lane 1), pcDNA3-H3.1-FLAG (lane 2), or pcDNA3-H3.3-FLAG (lane 3), and at 24 hpt, lysates were prepared and subjected to 15% SDS-PAGE, followed by Western blot analyses using anti-FLAG (top) and anti-β-actin (bottom) antibodies. (E) ChIP assays. HeLa cells transfected with the pcDNA3 empty vector (lanes 2, 3, 9, and 10), pcDNA3-H3.1-FLAG (lanes 4, 5, 11, and 12), or pcDNA3-H3.3-FLAG (lanes 6, 7, 13, and 14) were infected with HAdV5 at an MOI of 100. At 10 hpi (left, lanes 1 to 7) or at 12 hpi (right, lanes 8 to 14), ChIP assays were carried out by using anti-FLAG (lanes 3, 5, 7, 10, 12, and 14) and anti-HA (as a negative control) (lanes 2, 4, 6, 9, 11, and 13) antibodies. At 10 hpi, HU was added to block viral DNA replication. The immunoprecipitated DNAs were amplified by semiquantitative PCR using the indicated primer sets. PCR products were separated on a 7% polyacrylamide gel and visualized by staining with ethidium bromide (EtBr). Input DNAs (lanes 1 and 8) were purified from 0.5% of lysates of cells transfected with the empty vector.

and subjected to ChIP assays with an anti-FLAG antibody. As shown in Fig. 3A, the exclusive binding of H3.3 on viral chromatin was observed at all the regions that we tested, with a gradual increase as infection proceeded. This finding is consistent with data from a recent report of a helper-dependent Ad vector (HdAd) indicating that histone H3.3 is specifically deposited onto HdAd DNA by HIRA, an H3.3-specific histone chaperone (34). Since HdAd alone does not undergo its DNA replication, the chromatin state of HdAd may reflect that of wild-type Ad in early phases of infection (13, 34).

Next, we performed ChIP assays at 12 hpi to examine which H3 variant is deposited onto newly synthesized viral DNA (Fig. 3B). We found that histone H3.3 but not H3.2 was associated with viral chromatin at this time point, as observed in the early phases of infection. The expression levels of both H3 variants were comparable (Fig. 3C), and both variants were associated with cellular chromatin with a similar binding level (rRNA gene) (Fig. 3A and B). These findings strongly suggest that this result was not due to some technical issues. Furthermore, we obtained the same results by using FLAG-tagged histone H3.1 instead of H3.2 (Fig. 3D and E). Thus, these results suggest that replication-independent histone variant H3.3 is selectively deposited onto not only incoming but also newly synthesized viral DNA in infected cells.

Histones but not the transcription factor USF1 are excluded from the site of viral DNA replication. To further investigate the

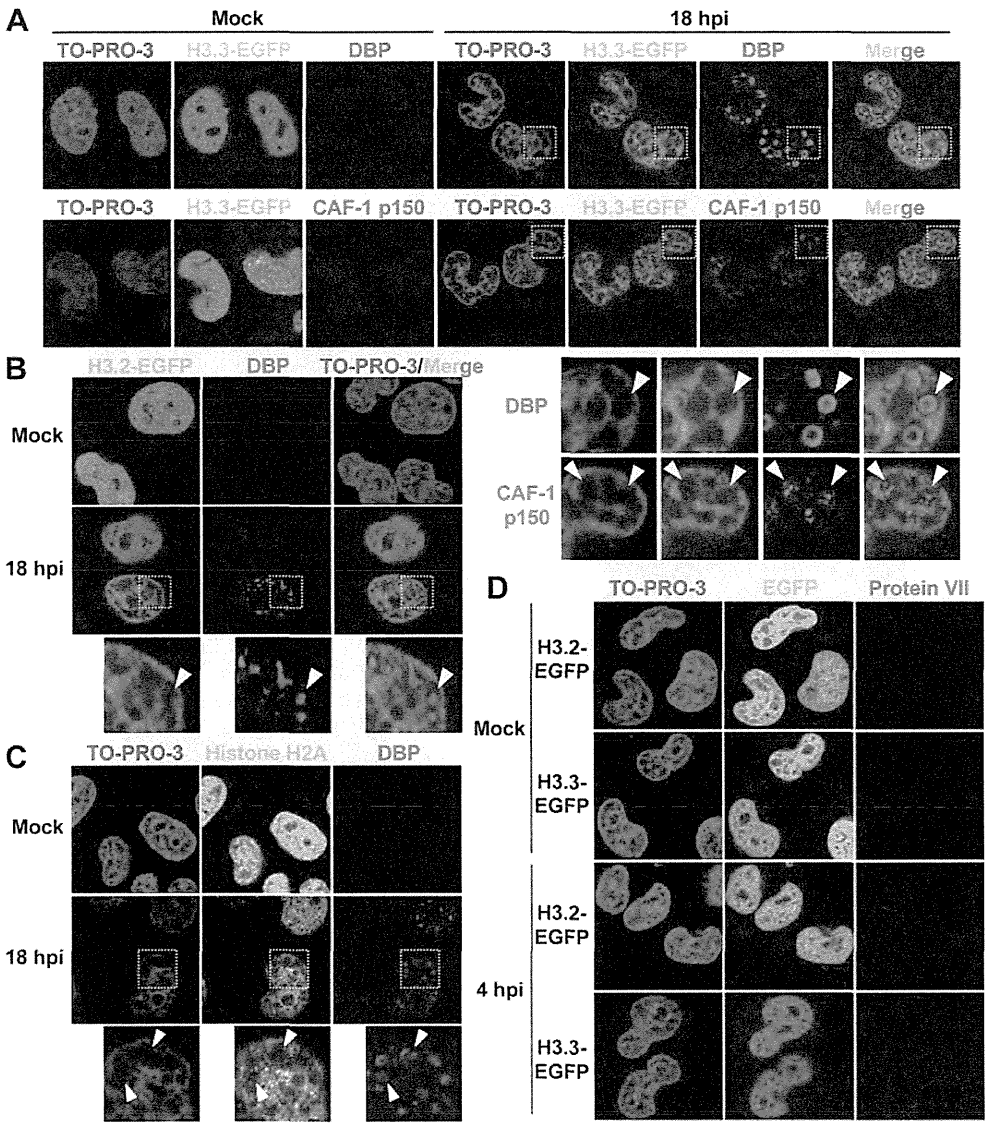

FIG 4 Localization of histones in late phases of infection. (A) IF analyses using cells stably expressing histone H3.3-EGFP. HeLa cells stably expressing histone H3.3-EGFP grown on coverslips were mock infected or infected at an MOI of 50, and at 18 hpi, the cells were subjected to IF assays using anti-DBP (top) and anti-CAF-1 p150 (bottom) antibodies. Higher-magnification images of the regions marked by squares are shown below. (B) Localization of histone H3.2 in late phases of infection. HeLa cells stably expressing histone H3.2-EGFP were mock infected or infected with HAdV5 at an MOI of 50, and at 18 hpi, the cells were subjected to IF analyses using an anti-DBP antibody. Higher-magnification images of the regions marked by squares are shown. (C) Localization of endogenous histone H2A in late phases of infection. HeLa cells were mock infected or infected with HAdV5 at an MOI of 50, and at 18 hpi, the cells were subjected to IF assays using anti-histone H2A and anti-DBP antibodies. Higher-magnification images of the regions marked by squares are shown below. (D) Histone localization in early phases of infection. HeLa cells stably expressing histone H3.2-EGFP and H3.3-EGFP were mock infected or infected with HAdV5 at an MOI of 250, and at 4 hpi, the cells were subjected to IF analyses using an anti-protein VII antibody.

fluctuation in histone levels during viral DNA replication, we performed IF analyses using HeLa cells stably expressing EGFP-tagged histone H3.3 (Fig. 4A). Cells were infected at an MOI of 50 and were subjected to IF assays using an anti-DBP antibody at 18 hpi (Fig. 4A, top). VDRF was observed at 18 hpi, as described above, and H3.3-EGFP was found to be excluded from VDRF. Similar results were obtained by using cells stably expressing EGFP-tagged histone H3.2 (Fig. 4B). This was due to neither exogenous expression nor the EGFP tag of H3 variants, as we observed a similar exclusion of the endogenous histone using anti-histone H2A antibody (Fig. 4C). This localization pattern was specific for the late phases of infection, since the localization of EGFP-tagged H3 variants was not changed in early phases of infection (Fig. 4D). We also performed IF analyses using anti-CAF-1 p150 antibody and observed that CAF-1 was accumulated at a "histoneless" region, that is, VDRF (Fig. 4A, bottom), as was observed for HA-PCNA (Fig. 2A). In summary, these results indi-